JOURNAL OF THE AERONAUTICAL SCIENCES

VOLUME 9 MAY, 1942 NUMBER 7

# The Control of Torsional Vibration in Radial Aircraft Engines by Means of Tuned Pendulums

VINCENT MOORE*

*Wright Aeronautical Corporation*

## Introduction

In 1936 Taylor[1] presented the fundamental theory of the tuned pendulum, or dynamic damper, as a means of controlling crankshaft torsional vibration. Since that time, the Wright Aeronautical Corporation has done extensive developing and testing of this device and has found it most effective. The dynamic damper has also been applied to the crankshaft of in-line engines with satisfactory results although the design problem for an in-line crankshaft is generally a more difficult one than for the usual single row radial engine crankshaft.

The success of the dynamic damper as applied to the radial aircraft engine has been so great that it leads many people to believe that it is a cure-all for torsional vibration problems and that at the first sign of difficulty it is only necessary to tack on a damper to overcome it. In general, however, the design of a suitable dynamic damper requires a careful study of the characteristics of the crankshaft-propeller system and the disturbing orders, in order to determine the location and the tuning of the necessary dampers to control the crankshaft vibration. It may be shown that the application of a damper to the shaft at some points will produce no improvement at all and that the indiscriminate application of a damper tuned to a prominent disturbing order may prove disastrous by building up a resonant condition with some other disturbing order acting on the system.

## Crankshaft-Propeller System

In Fig. 1 is shown a diagram of the crankshaft-propeller system of a typical single row radial aircraft engine. This type of crankshaft differs from an in-line engine crankshaft, most notably, in having only one crank throw. The connecting rods of all cylinders are linked to this throw and the effective mass of the pistons and connecting rods of the entire engine are concentrated on the single pin. The balance of the engine is achieved by means of counterweights fastened to the crank cheeks and it is apparent that the entire rotating masses of the power section of the engine are concentrated at this part of the shaft. At the propeller end of the system there is the large inertia of the propeller and in between the distributed inertia of the shafting and reduction gears. At the other end of the system are found the supercharger and accessories.

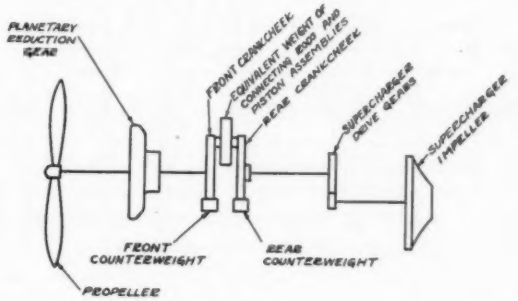


Fig. 1.

In general, such a system as described above has an infinite number of modes of vibration and an infinite number of natural frequencies. However, for purposes of analysis, the system will be simplified to the one shown in Fig. 2. In this system the supercharger and accessories have been neglected since they do not seriously influence the crankshaft vibration in the operating range.

This system is recognized, as far as twist in the shaft

Received February 3, 1942.

* Engineering Department.

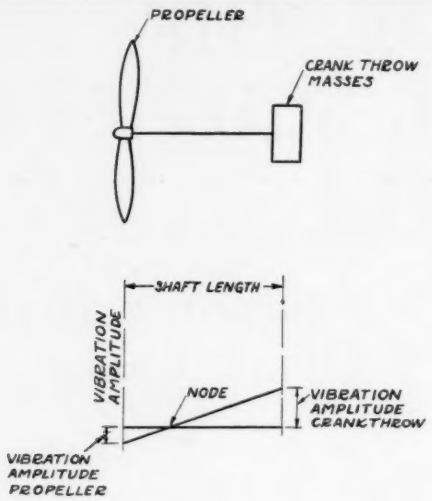


FIG 2.

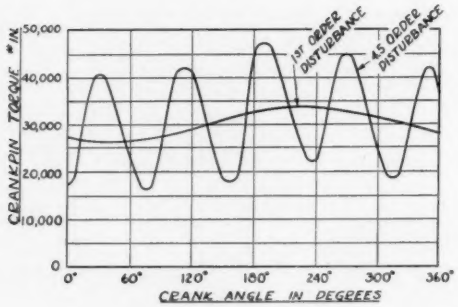


FIG. 3.

is concerned, as one having a single degree of freedom and, therefore, only one natural frequency. The calculated natural frequency of this system is very nearly equal to the measured value from actual engine test and it has also been found experimentally that this is the only resonant frequency which is of importance.

In an in-line engine it would not be legitimate to simplify the crankshaft to a single degree of freedom system because of the relatively uniform distribution of the masses along the shaft. In dealing with the simplified system of Fig. 2, conclusions are reached, however, which may be applied directly to a multinoded system and the application of a damper to an in-line shaft may be made by a suitable torsional analysis of the crankshaft without the damper attached.

## DISTURBING TORQUES

Fig. 3 shows the resulting torque acting upon the crankpin in a nine-cylinder single row radial engine. It is also possible that airflow interference may act upon the propeller and cause torsional vibrations but, to the writer's knowledge, this has never been found to be serious and will not be considered here. There are two prominent disturbing torques: (1) a first order disturbance arising from the master rod construction used in most radial engines; (2) the 4.5 order disturbance which is, of course, the firing frequency, since all nine cylinders fire every two revolutions of the crankshaft.

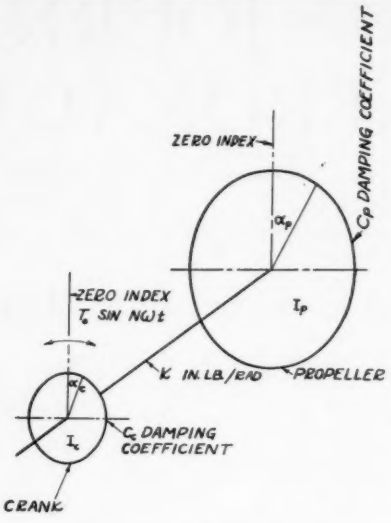


FIG. 4.

The order number is defined as the ratio of the frequency of the disturbance (or vibration) to the crankshaft speed.

## CRANKSHAFT MOTION

Before introducing the dynamic damper, it will be instructive to study the motion of the crankshaft system when acted upon by the torque shown in Fig. 3. The twist in the shaft produced by the mean torque will be constant and independent of engine speed. The variation in torque will produce a vibratory motion of the shaft and it will be convenient to consider this as made up of two components, a first order disturbance and a 4.5 order disturbance. From the solution of a general analysis for an $N$th order disturbance it is possible to describe the total motion of the shaft by taking the algebraic sum of its components. Now, with reference to Fig. 4, let

$I_p$ = propeller moment of inertia.
$I_c$ = crank mass moment of inertia.
$K$ = shaft constant, inch pounds per radian of twist of one disc relative to the other.
$T_0 \sin N\omega t$ = disturbing torque, in which $t$ is the time, $\omega$ is the angular velocity of the crankshaft in radians per sec., $N$ is the order of the disturbance, $T_0$ is the amplitude of the disturbance.
$\alpha_p$ = angular displacement of the propeller in radians.
$\alpha_c$ = angular displacement of the crank in radians.

In order to simplify the mathematics, damping is

neglected. Applying Newton's laws of motion to the propeller

$$0 = I_p\ddot{\alpha}_p + K(\alpha_p - \alpha_c) \tag{1}$$

and for the crank

$$T_0 \sin N\omega t = I_c\ddot{\alpha}_c - K(\alpha_p - \alpha_c) \tag{2}$$

from Eq. (1)

$$\alpha_c = (1/K)[I_p\ddot{\alpha}_p + K\alpha_p] \tag{3}$$

Solving these equations for the forced motion

$$\alpha_p = \frac{T_0 \sin N\omega t}{(I_p + I_c)\, N^2\omega^2[(N^2\omega^2/\gamma^2) - 1]} \tag{4}$$

$$\alpha_c = \left\{\frac{T_0 \sin N\omega t}{[I_p + I_c]\ [(N^2\omega^2/\gamma^2) - 1]}\right\}\left\{\frac{1}{N^2\omega^2} - \frac{1}{K/I_p}\right\} \tag{5}$$

where $\gamma = \{[K(I_p + I_c)]/[I_pI_c]\}^{1/2}$, the natural frequency of the system. The twist in the shaft is given by

$$(\alpha_p - \alpha_c) = \left\{\frac{T_0 \sin N\omega t}{[I_p + I_c]\ [(N^2\omega^2/\gamma^2) - 1]}\right\}\left\{\frac{1}{K/I_p}\right\} \tag{6}$$

Eqs. (4), (5), and (6) are plotted in Fig. 5 for a typical nine-cylinder radial engine of the geared type, having an output of approximately 1,000 hp.

$I_p$ = 172.5 lbs. in. sec.$^2$
$I_c$ = 12.84 lbs. in. sec.$^2$
$K$ = 0.494 × $10^7$ lbs. in. rad.
$T_0$ = 10,000 lbs. in.

$T_0$ has been taken as constant for all speeds; actually, of course, the disturbing torque will vary with the b.m.e.p. of the engine. If it is desired to obtain vibration amplitudes corresponding to some different torque variation (say, $T_0'$) these may be obtained from the curves by multiplying the plotted amplitudes by the ratio of $T_0'/T_0$. Thus the curves of Fig. 5 are general in form.

The most prominent feature of the curves is the resonant point at 1,360 r.p.m. At this point, and for considerable range on either side, the vibration amplitude and twist in the shaft become large. Experience has shown that even small vibrational disturbances may produce dangerous stresses in a metal propeller.

The vibratory motion of the whole system is limited by the total damping so that the vibration amplitudes never actually become infinite. However, at resonance the vibration may build up until the twist in the shaft becomes 15 to 20 times the static twist. The resulting high stresses are destructive to the crankshaft and reduction gear system and the large amplitudes at the accessory drive coupling play havoc with the supercharger and accessory drive gears.

From the standpoint of the engine alone, the removal of the resonant point from the operating range would be a satisfactory solution to the vibration problem. However, this would not be sufficient to make feasible the driving of all metal propellers and some other means

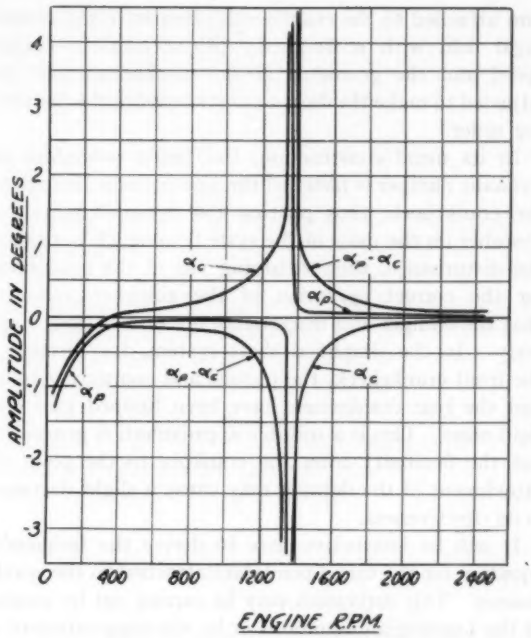


FIG. 5.

must be provided to further reduce the crankshaft vibration.

In Fig. 5, note that $\alpha_c$ has a zero value at 360 r.p.m. At this speed the twist in the shaft is finite and given by Eq. (6), which may be reduced as follows:

$$\alpha_p - \alpha_c = [T_0 \sin N\omega t]/[(N^2\omega^2 - \gamma^2)I_c]$$

Now for $\alpha_c = 0$, $(1/N^2\omega^2) - (I_p/K) = 0$ from Eq. (5) and $N^2\omega^2 = K/I_p$. Therefore

$$\alpha_p - \alpha_c = \frac{T_0 \sin N\omega t}{[(K/I_p) - \gamma^2]I_c} = -\frac{T_0}{K}\sin N\omega t$$

The conditions for $\alpha_c$ to be zero at 360 r.p.m. are as follows:

(1) The disturbing frequency $N\omega = (K/I_p)^{1/2}$ equals the natural frequency of the propeller-crankshaft system when vibrating with a node at the crank.

(2) The amplitude of the twist in the shaft is $-(T_0/K)$. This corresponds to the static twist which would be produced by a steady torque of value $T_0$.

These conditions are immediately recognized as those for an undamped dynamic vibration absorber applied to a torsional system.[2]

As Den Hartog points out, a fixed frequency dynamic vibration absorber is only useful when the machinery to which it is attached is acted upon by a fixed frequency disturbance to which the damper may be tuned. In an internal combustion engine, the disturbing torque frequencies vary with engine speed so that a dynamic vibration absorber, to be useful, must have a natural frequency which also varies with engine speed in such a way that the absorber frequency remains equal to the disturbing frequency. As shown by Taylor,[1] a pendu-

lum attached to the crankcheek vibrates in the centrifugal field with a frequency proportional to engine speed and the geometry of the mechanism may be adjusted to make the damper order equal to the disturbing order.

In its usual construction, the tuned pendulum or dynamic damper is fastened through suitable linkage to the crankcheek, thus putting the dynamic vibration absorber on the mass of the system to which is applied the disturbance, thus satisfying one of the conditions for the correct operation of the absorber—namely, that the damper and disturbance act on the same rigid body. In the simplified shaft system, the inertia of the front crankcheek, the pistons and connecting rods, and the rear crankcheek have been lumped into one rigid mass. This is a suitable approximation generally, but the flexibility from the crankpin to the point of attachment of the damper may cause a slight decrease in its effectiveness.

It will be instructive here to derive the frequency equation for the tuned pendulum attached to the crank masses. This derivation may be carried out by means of the Lagrangian equations or by the supposition of a centrifugal field of force. However, both of these methods involve a great deal of algebra and also obscure the fundamental forces acting on the damper and its support. The writer prefers a third method that reduces the algebra to a minimum and, at the same time, gives a complete vector diagram showing the accelerations and, therefore, the forces acting on pendulum mass. This method also has the advantage of permitting the building up of a solution for more complicated arrangements of the damper by going back to the original vector diagram and making the necessary additions to the acceleration vector.

### The Tuned Pendulum

Fig. 6 shows a disc to which is attached a simple pendulum of length $l$. The axis of rotation of the disc is $O$ and the pendulum pivot is located a distance $q$ from $O$. This diagram is correlated with engine construction. The disc corresponds to the crank throw masses, $O$ is the shaft center, and the pendulum is the dynamic damper.

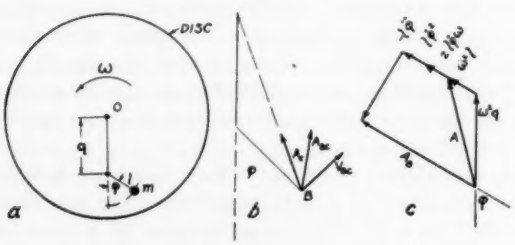


Fig. 6.

What will the vibratory motion of the pendulum be when the disc rotates at uniform speed and the pendulum is disturbed from its equilibrium position? That the pendulum will vibrate about its equilibrium position is obvious but it is not so obvious just what its frequency will be.

In order to determine the natural frequency the following is noted.

(1) The link $l$ is the only body in contact with the mass $m$. The supposition of a simple pendulum gives a mass $m$ which has zero moment of inertia about its c.g. The link $l$, therefore, can apply on $m$ only a push or pull which lies along $l$.

(2) The absolute acceleration of $m$ will have the same direction as the resultant force acting on $m$ and, since there are no force fields present (gravity neglected), the absolute acceleration of $m$ lies along the link $l$.

Let the absolute acceleration of $m$ be denoted by $A_B$. Then $A_B = A_C + A_{BC} + 2V_{BC}\omega$, where vector addition is understood and

$A_C$ = absolute acceleration of the point on the disc with which $m$ coincides at the instant in question.

$A_{BC}$ = relative acceleration of $m$ with respect to the point on the disc with which it coincides at the instant in question.

$V_{BC}$ = velocity of $m$ relative to the point on the disc with which it coincides at the instant in question.

$\omega$ = angular velocity of the disc at the instant in question.

$A_{BC} = l\dot{\varphi}^2 + l\ddot{\varphi}$ vector addition.

$V_{BC} = l\dot{\varphi}$

$A_C = \omega^2 q + \omega^2 l$ vector addition.

In Fig. 6 the vector addition is shown. Note that the closing side of the diagram must be plotted opposite the positive direction of $\ddot{\varphi}$. With the motion of $m$ perpendicular to $l$, then $-l\ddot{\varphi} = \omega^2 q \sin \varphi$.

Now for small values of $\varphi$: $\sin \varphi \approx \varphi$ and $\ddot{\varphi} + (\omega^2 q/l)\varphi = 0$.

This is immediately recognized as the differential equation for simple harmonic motion with a frequency

$$P = \sqrt{\omega^2(q/l)} = \omega \sqrt{q/l} \tag{7}$$

Note that the pendulum frequency is directly proportional to engine speed. The pendulum, therefore, has the desired property that its natural frequency varies directly with engine speed. It is only necessary to choose $q$ and $l$ to fix the ratio at the desired engine order.

Eq. (7) may be rewritten as

$$\frac{P}{\omega} = \Omega = \sqrt{q/l} \text{ cycles per revolution} \tag{8}$$

where $\Omega$ is the pendulum order.

It may be shown that the same general property holds in the case of a compound pendulum except that the polar moment of inertia of the pendulum mass must be considered. In applying the foregoing equations to an

actual case where the pendulum order is relatively high (4.5 for a nine-cylinder engine), it is found that the ordinary compound pendulum construction is not feasible because of the excessive moment of inertia of any mass large enough to do an effective job of vibration absorption. To overcome this difficulty, R. Chilton has brought out the design shown in Fig. 7a. The bifilar construction eliminates the relative angular motion of the pendulum and, therefore, nullifies the effect on frequency of its moment of inertia. The actual Chilton construction is as shown in Fig. 7b. The

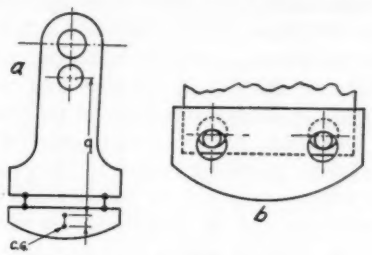


FIG. 7

bushings are all of the same diameter and it is obvious that the pendulum length $l$ is given by the difference between the bushing diameter and the pin diameter. This construction also gives a pure rolling motion which is very desirable, since ideally, the damper should be frictionless. In the damper construction shown in Fig. 7b, note that the pin motion is not that of a simple pendulum. The effect of the pins on the damper tuning is shown in the following equation.

$$\Omega^2 = \frac{mq + m_p G}{2(b-a)\{m + (m_p/2)[1 + (\rho^2/a^2)]\}} \tag{9}$$

where

$m$ = mass of damper.
$m_p$ = mass of one pin.
$\rho$ = radius of gyration of the pin about its own axis.
$G$ = distance from crankshaft axis to the common center line of the crankcheek damper bushings. Bushings assumed symmetrically disposed about damper c.g.
$q$ = distance from crankshaft axis to center of oscillation of c.g. of $m$.
$b$ = bushing radius.
$a$ = pin radius.
$\Omega$ = damper order.

Note that this reduces to 8 when $m_p = 0$. Then, $\Omega^2 = q/l$, since $2(b - a) = l$, the pendulum length.

For the usual values of $m$, $m_p$, and $\rho$ the effect of the roller on damper frequency is negligible and in damper calculations it is generally neglected.

With the above equations, it is possible to specify the the exact geometric relationship that must exist to produce proper damper tuning. However, because of manufacturing tolerances and crankshaft flexibility, it is not possible to accomplish exact tuning. As the first move in determining how accurately the damper must be constructed, it will be of interest to know to what extent detuning of the damper will affect its efficiency and the resulting crankshaft vibration.

## VIBRATORY AMPLITUDE AS INFLUENCED BY DAMPER TUNING

It is not necessary to think of any one particular design of damper for the general treatment of the crankshaft vibration. As far as the damper motion is concerned, however, it is obvious that this will be dependent on the damper type. In general, however, the interest is only in whether the damper amplitude becomes large, regardless of what its form may be.

If the system of Fig. 2 is considered and a tuned pendulum is attached to the crank masses, the following equations of motion are obtained:

For the damper, $-m(l\ddot{\varphi} + R\ddot{\alpha}_c) = m\omega^2 q\varphi$, where $R = q + l$.

For the crank, $I_c\ddot{\alpha}_c - K(\alpha_p - \alpha_c) - mR\omega^2 q\varphi = T_0 \sin N\omega t$.

For the propeller, $0 = I_p\ddot{\alpha}_p + K(\alpha_p - \alpha_c)$.

The forced vibration of the system will be of the form

$$\alpha_c = a_1 \sin N\omega t$$
$$\varphi = a_2 \sin N\omega t$$
$$\alpha_p = a_3 \sin N\omega t$$

Substituting these values and letting $e = T_0/K$ = the static twist in crankshaft; $\omega_c = \sqrt{K/I_c}$ = the natural frequency of the crank masses, oscillating with a node at the propeller; and $\omega_p = \sqrt{K/I_p}$ = the natural frequency of the propeller oscillating with a node at the crank masses

$$\frac{a_1}{e} = \frac{1}{\left[1 - \frac{N^2\omega^2}{\omega_c^2} - \frac{1}{1 - (N^2\omega^2/\omega_p^2)}\right] - \left[\frac{mR^2N^2\omega^2}{K}\left(\frac{\Omega^2}{\Omega^2 - N^2}\right)\right]} \tag{10}$$

$$\frac{a_2}{e} = \frac{R/l[N^2/(\Omega^2 - N^2)}{\left[1 - \frac{N^2\omega^2}{\omega_c^2} - \frac{1}{1 - (N^2\omega^2/\omega_p^2)}\right] - \left[\frac{mR^2N^2\omega^2}{K}\left(\frac{\Omega^2}{\Omega^2 - N^2}\right)\right]} \tag{11}$$

$$\frac{a_3}{e} = \frac{1/[1 - (N^2\omega^2/\omega_p^2)]}{\left[1 - \frac{N^2\omega^2}{\omega_c^2} - \frac{1}{1 - (N^2\omega^2/\omega_p^2)}\right] - \left[\frac{mR^2N^2\omega^2}{K}\left(\frac{\Omega^2}{\Omega^2 - N^2}\right)\right]} \tag{12}$$

Note that the denominators are all equal. When the denominator equals zero there are infinite amplitudes.

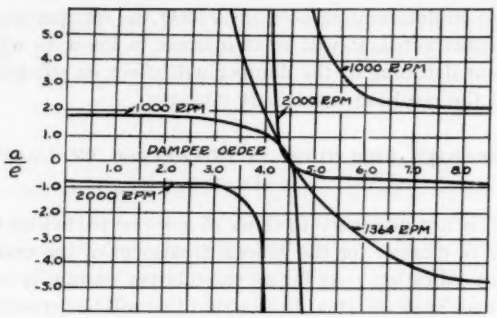


FIG. 8.

This gives the natural frequency equation, which is

$$\left[1 - \frac{N^2\omega^2}{\omega_c^2} - \frac{1}{1-(N^2\omega^2/\omega_p^2)}\right] - \left[\frac{mR^2N^2\omega^2}{K}\left(\frac{\Omega^2}{\Omega^2 - N^2}\right)\right] = 0$$

In order to simplify this equation multiply through by $[1 - (N^2\omega^2/\omega_p^2)]$.

Multiplying out and canceling like terms,

$$-N^2\omega^2\left[\frac{1}{\omega_p^2} + \frac{1}{\omega_c^2} + \frac{mR^2}{K}\left(\frac{\Omega^2}{\Omega^2 - N^2}\right)\right] + N^4\omega^4\left[\frac{1}{\omega_c^2\omega_p^2} + \frac{1}{\omega_p^2}\left(\frac{mR^2}{K}\right)\left(\frac{\Omega^2}{\Omega^2 - N^2}\right)\right] = 0$$

Now divide by $N^2\omega^2$, which gives us a root $N^2\omega^2 = 0$ as a resonant frequency. Although this is theoretically correct, it is a trivial solution and will be neglected. After dividing, rearranging terms, and solving for $N^2\omega^2$

$$N^2\omega^2 = \frac{1 + \frac{\omega_p^2}{\omega_c^2} + \left(\frac{\omega_p^2\Omega^2}{\Omega^2 - N^2}\right)\frac{mR^2}{K}}{\frac{1}{\omega_c^2} + \left(\frac{\Omega^2}{\Omega^2 - N^2}\right)\frac{mR^2}{K}} \qquad (13)$$

This equation may be readily checked at $\Omega^2 = 0$, which corresponds to no damper at all, and at $\Omega^2 = \infty$, which corresponds to the damper rigidly fastened to the crankcheek.

For $\Omega^2 = 0$

$$N^2\omega^2 = \omega_c^2 + \omega_p^2 = \frac{K}{I_c} + \frac{K}{I_p} = K\frac{(I_p + I_c)}{I_pI_c}$$

which is as it should be, for $\Omega^2 = \infty$

$$N^2\omega^2 = \frac{\omega_c^2 + \omega_p^2 + \omega_c^2\omega_p^2(mR^2/K)}{1 + (\omega_c^2 mR^2/K)} = K\frac{I_p + (I_c + mR^2)}{I_p(I_c + mR^2)}$$

which is also as it should be since infinite-damper tuning is equivalent to adding inertia equal to $mR^2$ to the crankcheek inertia $I_c$.

From Eqs. (10), (11), and (12) the vibration amplitudes of the crankcheek damper and propeller as a function of damper tuning may be determined.

In Fig. 8 are plotted curves showing the effect of detuning for three different engine speeds. Although the plotted values are for the motion of the crank masses only, the motions of the damper and propeller may be obtained from these curves and Eqs. (11) and (12). The crankshaft propeller system is the same as the system used for Fig. 5.

The curve for 1,364 r.p.m. shows that corresponding to this engine speed the damper order must be reduced to zero if resonance is to be obtained. It is obvious what this resonance is, since zero damper tuning corresponds to no damper at all and with no damper resonance at the natural frequency of the shaft system must be expected. As the damper order is increased it is equivalent to adding inertia to the crank masses until 4.5 order is reached, at which point the added inertia is infinite and the amplitudes are zero. Above 4.5 order the effective inertia becomes finite again and shaft amplitudes increase until at infinite damper order there are amplitudes corresponding to the damperless system, with the addition to the crankshaft masses of inertia equal to $mR^2$.

At speeds below the damperless resonant speed the amplitudes are represented by the curve for 1,000 r.p.m. The amplitude changes very slowly as the damper order increases from zero to about four. Above this value the damper takes over and rapidly reduces the amplitude to zero as 4.5 order is reached. Above 4.5 order the amplitude increases very rapidly until resonance is reached at 4.84 order. Above this value the amplitude becomes finite again and decreases to about two times the static twist as the damper tuning approaches infinity.

At 2,000 r.p.m. the curve is similar to that for 1,000 r.p.m. but with a reversal in sign and shift of the resonance point to an order below 4.5.

It is clear from these curves that larger errors in damper tuning will have considerable effect on the vibratory response. In actual practice, however, it is not difficult to obtain tuning very nearly equal to 4.5. Manufacturing tolerances may change the damper tuning from 4.5 to 4.45 or 4.55, but it is obvious, at least for the plotted curves, that this slight tuning error will not be serious.

Fig. 9 shows vibration amplitudes plotted against engine r.p.m. for varying degrees of damper tuning.

It is to be noted that the vibration amplitudes become very large near zero r.p.m. These large amplitudes represent the motion of the crankshaft and propeller as a rigid body and do not correspond to large twist in the crankshaft. In actual practice they will be of no importance since the disturbing torque will be very small at low engine speeds and no appreciable amplitude will exist. As the r.p.m. reaches 360, the propeller acts as a dynamic vibration absorber for the

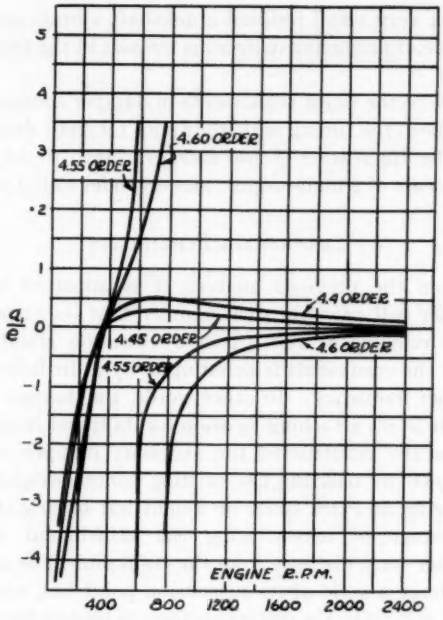


FIG. 9.

crankshaft, as is noted in the discussion on "Crankshaft Motion," and this, of course, necessitates some vibratory motion of the propeller. The propeller will vibrate to balance the disturbing torque leaving the crankcheek and damper at rest. This point, although of academic interest, is of little practical importance because of the low engine speed.

The next significant feature is the resonant effect for "high" tuning and the absence of this for "low" tuning. Fig. 10 shows the spectrum of resonant speeds plotted against damper tuning. As explained before, the end points correspond to no damper at all and the damper rigidly clamped to the cheek for the zero and infinite orders, respectively. Over most of the range the resonant speeds are nearly equal, but between 3.5 and 5.0 they change greatly. At 4.23 order the resonant speed is infinite and between 4.23 and 4.48 there are no resonant speeds at all. As the damper tuning increases from 4.48 the resonant speeds rapidly increase from zero to about 1,100 r.p.m. at fifth order. Above fifth order the change is gradual with the limiting condition corresponding to infinite damper tuning being approached asymptotically.

Looking back at Fig. 9 it is apparent that above 1,200 r.p.m. there is little to choose between a tuning error that is high or one that is low. Below 1,200 r.p.m. engine operation is so infrequent and of such low power that the resonant points noted are of little practical importance.

### VIBRATORY AMPLITUDES AS INFLUENCED BY DISTURBING FREQUENCY

In Figs. 8, 9, and 10, it was found that for any given disturbing frequency vibration amplitudes may be-

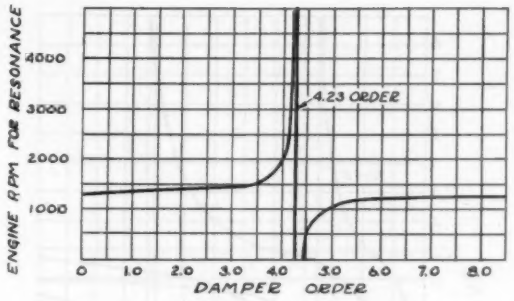


FIG. 10.

come larger as the damper tuning changes. It is not difficult to imagine that for a given damper tuning resonant points will appear as the disturbing order is changed.

Consider the resonant frequency Eq. (13); let the damper tuning be 4.5 order and solve for $\omega$ with $N$ varying.

$$\omega^2 = \frac{107 + \left(\frac{20.25}{20.25 - N^2}\right)}{7.40 + \left(\frac{20.25}{20.25 - N^2}\right)} \left(\frac{0.0286 \times 10^6}{N^2}\right)$$

$$\omega_{\text{r.p.m.}} = \left[\frac{107 + \frac{20.25}{20.25 - N^2}}{7.40 + \frac{20.25}{20.25 - N^2}}\right]^{1/2} \left(\frac{1615}{N}\right) \qquad (14)$$

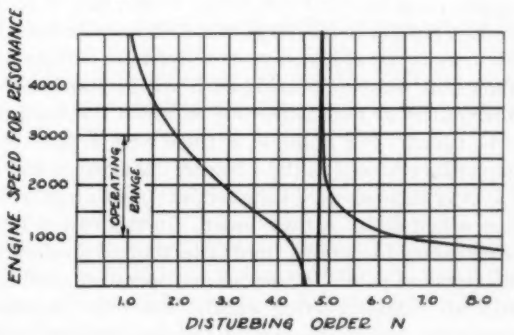


FIG. 11.

Eq. (14) has been plotted in Fig. 11, but before examining this curve investigate a few specific disturbing orders, that might be present in a nine-cylinder four-stroke cycle radial engine. The most prominent disturbance is, of course, the 4.5 order, but this has already been investigated. Due to the articulated rod construction there is an appreciable first order torque variation and misfiring of a cylinder will introduce a 0.5 order disturbance as well as higher harmonics. There may also be some ninth order torque variation, so consider the following orders 0.5, 1, 3, and 9 and plot curves showing vibration amplitudes against engine r.p.m.

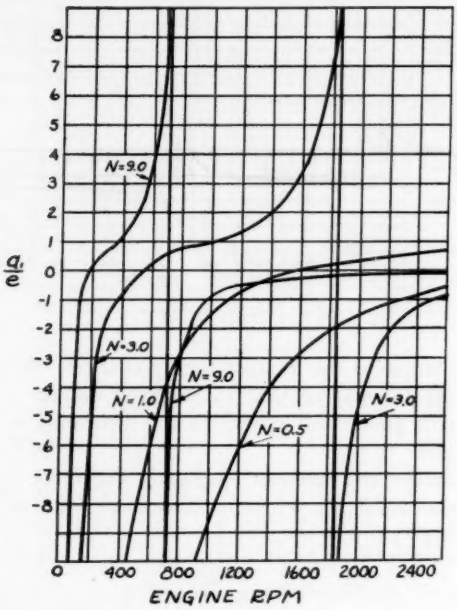


FIG. 12.

In Fig. 12, Eq. (10) has been plotted for a range of disturbing orders from the lowest possible order (0.5 order) to the highest order of any consequence (ninth order) for damper tuning of 4.5.

In Fig. 10 the operating range of the engine has been shown as 1,000 to 3,000 r.p.m. Within this range the engine orders from 1.9 to 4.25 and from 4.82 to 6.45 will produce resonance and large vibration amplitudes. For this reason the application of a dynamic damper to a crankshaft must be considered from the standpoint of other orders as well as the one to which the damper is to be tuned. For example, if there were a third order disturbance as well as the 4.5 order disturbance and the 4.5 order damper were installed, at 1,840 r.p.m. resonance would occur at third order. In this case it might be necessary to install a third order damper to eliminate this resonant point. Under normal operating conditions with all cylinders firing evenly, the only prominent disturbing orders present in a nine-cylinder radial engine are the first order and the 4.5 order. The 4.5 order is controlled by the damper and the first order resonance point lies far above the operating range. It would be expected, therefore, that a damper installation in a nine-cylinder radial engine would be 4.5 order and that no troublesome torsional vibration conditions would occur in the operating range. In general this has been found to be the case as far as crankshaft stresses are concerned, but some trouble has been encountered with propeller vibration. In this analysis so far, the effects of friction on the damper action and the flexibility of the crankcheek to which the damper is attached have been neglected. These two factors are negligible where crankshaft stress only is concerned but are of importance when propeller vibration is considered, since a very small residual crankshaft vibration seems capable of producing dangerous stresses in the propeller blades.

Two of the latest refinements in damper construction have been the tuning with allowance for shaft flexibility and the application of two dampers tuned to 4.5 order in the case of a high-output, nine-cylinder radial engine.

## CRANKSHAFT FLEXIBILITY

From the previous analysis it is apparent that a damper will swing in such manner that its suspension point remains at rest (from a vibration standpoint) when the crankshaft is acted upon by a disturbance of damper frequency. In other words, the damper forces a node at its attaching location for its tuned frequency. As usually constructed the necessary damper mass is obtained by utilizing the existing counterweight, thus requiring no extra space or weight but having the disadvantage of necessitating the attachment of the damper some distance from the crankpin. The damper will force a node at its suspension point but, since the shaft is flexible, the disturbing force acting on the crankpin will produce some vibratory twist in the shaft. In forcing a node at the rear cheek, the natural frequency of the crankshaft propeller system is lowered to that of the propeller vibrating against the rear cheek of the crankshaft as a fixed point. This natural frequency is low, corresponding to 360 r.p.m. for the 4.5 order disturbance, and the friction effects will be very large compared to the disturbing effect, since the disturbance acts at a point close to a node and the damping acts where the amplitude is large. Because of this and also because the resonant speed is below the operating range, this resonant vibration is of no importance. In the operating range the shaft amplitudes will be small but propeller vibration may be destructive, and for high output engines it becomes necessary to change the damper tuning so as to produce a node at the crankpin rather than at the rear cheek. Adjusting the damper tuning to produce a node at the crankpin is, of course, equivalent to attaching a damper to the crankpin, and this is exactly what is desired, since the theory indicates that for complete vibration elimination it is only necessary to attach the damper system to the main system at the point of application of the disturbing force.

The damper order necessary to produce a node at the center of the crank has been shown by Taylor[3] to be given by the following equation:

$$P^2 = \frac{\Omega^2[(S^2/\Omega^2) - 1]}{[(S^2/\Omega^2) - 1 - (mR^2/I_{cs})]} \qquad (15)$$

$P$ is equal to the natural frequency of the damper as determined by its pendulum length and center of oscillation, $S$ is the natural frequency of the cheek vibrating with a node at the crankpin center, and $\Omega$ equals 4.5 order or the desired order for the damper and cheek system.

In applying Eq. (15) to the crankshaft dealt with in previous chapters, it is practically impossible to calculate accurately either $T_1$ or $I_{cs}$.

Taylor has calculated $T_1$ by assuming the shaft rigidity to be equivalent to a section of crankpin which extends from the center of the pin half way into the crankcheek.

The writer has calculated the rigidity by using the methods shown by Timoshenko.[4] Approximations are made in this analysis also so that there is still some doubt as to the absolute accuracy of the results, but it will be of interest to see what order of magnitude results for the change in damper tuning.

$I_{cs} = 2.59$ lbs. in. sec.$^2$
$mR^2 = 1.64$ lbs. in. sec.$^2$
$T_1 = 59.3 \times 10^6$ lbs. in./rad.
$\Omega^2 = 0.223\ N_e^2$, $N_e$ = engine r.p.m.
$\frac{mR^2}{I_{cs}} = 0.632$
$S^2 = (59.3 \times 10^6)/2.59 = 22.9 \times 10^6$

For practical interpretation evaluate $P$ in terms of the change in pendulum length, which is given by

$$-\Delta l = \frac{q}{20.25}\left[1 - \frac{(mR^2/I_{cs})}{(S^2/\Omega^2) - 1}\right] - \frac{q}{20.25}$$

$$\Delta l = \frac{0.169}{[(S^2/\Omega^2) - 1]}$$

This equation is plotted in Fig. 13.

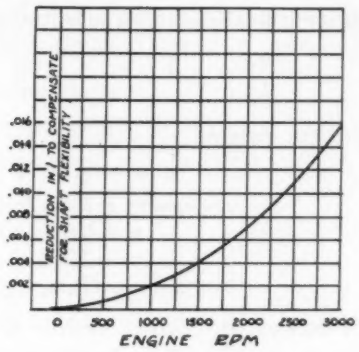


FIG. 13.

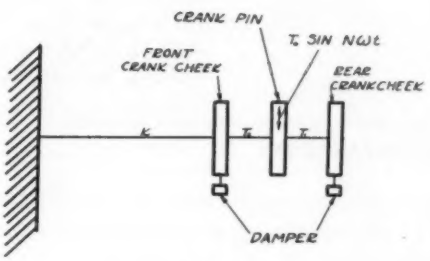


FIG. 14.

From actual measurements it has been found that shortening the pendulum length 0.005 in. gives a reduction in propeller stresses when the damper is mounted on the rear crankcheek. This seems to be in good agreement with the calculated values, at least from the standpoint of order of magnitude.

It should be noted that any one value of pendulum length is correct at one speed only and the choice of a satisfactory $l$ will depend on vibration measurements to determine at what speeds propeller stresses are high.

The quantitative side of the problem of tuning the damper high to compensate for shaft flexibility is one best approached with experimental, rather than analytical, methods.

It should be noted that in pushing the node forward to the center of the crankpin the vibratory motion of the rear cheek has been increased and that vibration measurements taken on the rear end of the crankshaft would be misleading if they were not properly interpreted.

### Double Damper Crankshaft

Another system for reducing propeller stresses consists of the addition of a second damper on the front crankcheek.

Fig. 14 shows schematically the system to be treated here. In order to simplify the mathematics as much as possible the following assumptions have been made:

$I_1 = I_2 = I_3 = I_c$
$m_1 = m_2 = m$
$R_1 = R_2 = R$ approx.
$q_1 = q_2 = q$

$I_p$ is infinite, giving a node at the forward end of the shaft

The last assumption is not justifiable at low shaft speeds, but within the operating range of the engine it is very nearly correct.

Since it is apparent that there is considerable uncertainty in the relative action of two frictionless dampers tuned to the same frequency and attached to the same "main mass," some friction within the damper itself will be included. If this is considered as viscous friction additional forces are as follows: acting on the crankcheek, $c_1 l\dot{\varphi}$; acting on the damper, $-c_1 l\dot{\varphi}$.

Including these forces the equations of motion become: for the rear cheek

$$I_c\ddot{\epsilon} = -T_1(\epsilon_1 - \epsilon_2) + mR\omega^2 q\varphi_1 + c_1 l_1\dot{\varphi}R \quad (16)$$

For the rear damper

$$ml_1\ddot{\varphi}_1 = -m\omega^2 q\varphi_1 - mR\ddot{\epsilon}_1 - c_1 l_1\dot{\varphi}_1 \quad (17)$$

For the crankpin

$$I_c\ddot{\epsilon}_c = T_1(\epsilon_1 - \epsilon_c) + T_2(\epsilon_2 - \epsilon_c) + T_0 \sin N\omega t \quad (18)$$

For the front cheek

$$I_c\ddot{\epsilon}_2 = -T_2(\epsilon_2 - \epsilon_c) + mR\omega^2 q\varphi_2 + c_2 l\dot{\varphi}_2 R - K\epsilon_2 \quad (19)$$

For the front damper

$$ml_2\ddot{\varphi}_2 = -m\omega^2 q\varphi_2 - mR\ddot{\epsilon}_2 - c_2 l_2\dot{\varphi}_2 \quad (20)$$

For simplicity make the following substitutions

$$\frac{I_1}{I_c} = S_1^2 \qquad \frac{\omega^2 q}{l_{1,2}} = p_{1,2}^2 \qquad \frac{T_2}{I_c} = S_2^2 \qquad \frac{K}{I_c} = S_3^2 \qquad \frac{mRl_1}{I_c} = Q_1^2 \qquad \frac{mRl_2}{I_c} = Q_2^2$$

and the equations become

$$\begin{aligned}
\ddot{\epsilon}_1 &= -S_1^2(\epsilon_1 - \epsilon_c) + Q_1^2 P_1^2 \varphi_1 + (c_1/m) Q_1^2 \dot{\varphi}_1 \\
\ddot{\varphi}_1 &= -P_1^2 \varphi_1 - (R/l_1)\ddot{\epsilon}_1 - (c_1/m)\dot{\varphi}_1 \\
\ddot{\epsilon}_c &= S_1^2(\epsilon_1 - \epsilon_c) + S_2^2(\epsilon_2 - \epsilon_c) + (T_0/I_c) \sin N\omega t \\
\ddot{\epsilon}_2 &= -S_2^2(\epsilon_2 - \epsilon_c) + Q_2^2 P_2^2 \varphi_2 + (c_2/m) Q_2^2 \dot{\varphi}_2 - S_3^2 \epsilon_2 \\
\ddot{\varphi}_2 &= -P_2^2 \varphi_2 - (R/l_2)\ddot{\epsilon}_2 - (c_2/m)\dot{\varphi}_2
\end{aligned} \tag{21}$$

These five differential equations describe the motion of the system. Since there is interest only in the forced motion, $\varphi_1$, $\varphi_2$, $\epsilon_1$, $\epsilon_2$, and $\epsilon_c$ will be harmonic motions of frequency $N\omega$ and the complex notation may be employed

$$\begin{aligned}
-N^2\omega^2\epsilon_1 &= -S_1^2(\epsilon_1 - \epsilon_c) + Q_1^2 P_1^2 \varphi_1 + \iota N\omega (c_1/m) Q_1^2 \varphi_1 \\
-N^2\omega^2\varphi_1 &= P_1^2 \varphi_1 + (R/l) N^2\omega^2 \epsilon_1 - \iota N\omega (c_1/m)\varphi_1 \\
-N^2\omega^2\epsilon_c &= S_1^2(\epsilon_1 - \epsilon_c) + S_2^2(\epsilon_2 - \epsilon_c) + (T_0/I_c) \\
-N^2\omega^2\epsilon_2 &= -S_2^2(\epsilon_2 - \epsilon_c) + Q_2^2 P_2^2 \varphi_2 + \iota N\omega (c_2/m) Q_2^2 \varphi_2 - S_3^2 \epsilon_2 \\
-N^2\omega^2\varphi_2 &= -P_2^2 \varphi_2 + (R/l_2) N^2\omega^2 \epsilon_2 - \iota N\omega (c_2/m)\varphi_2
\end{aligned} \tag{22}$$

Solving these equations

$$\epsilon_c = \frac{T_0/I_c}{\left[(-N^2\omega^2 + S_1^2 + S_2^2) - \dfrac{S_1^4}{(-N^2\omega^2 + S_1^2) - \dfrac{Q_1^2\left(P_1^2 + \iota N\omega \dfrac{c_1}{m}\right)(R/l_1)N^2\omega^2}{\left(-N^2\omega^2 + P_1^2 + \iota N\omega \dfrac{c_1}{m}\right)}} - \dfrac{S_2^4}{(-N^2\omega^2 + S_2^2 + S_3^2) - \dfrac{Q_2^2\left(P_2^2 + \iota N\omega \dfrac{c_2}{m}\right)(R/l_2)N^2\omega^2}{\left(-N^2\omega^2 + P_2^2 + \iota N\omega \dfrac{c_2}{m}\right)}}\right]} \tag{23}$$

This equation provides a convenient solution for $\epsilon_c$ when all the physical characteristics of the system are known. However, it is hardly suitable for a general analysis so its use can be avoided by splitting the general problem into two separate problems. First, consider that $S_1$ and $S_2$ are so large that any twist in the shaft between the crankpin and the crankcheeks may be neglected, then $\epsilon_1 = \epsilon_2 = \epsilon$. This is equivalent to the lumped moments of inertia which have been considered before but with the addition of the second damper. The equilibrium equations become

$$\begin{aligned}
\ddot{\epsilon}_c &= Q_1^2 P_1^2 \varphi_1 + (c_1/m) Q_1^2 \dot{\varphi}_1 + Q_2^2 P_2^2 \varphi_2 + (c_2/m) Q_2^2 \dot{\varphi}_2 - S_3^2 \epsilon_c + (T_0/I_c) \sin N\omega t \\
\ddot{\varphi}_1 &= -P_1^2 \varphi_1 - (R/l_1)\ddot{\epsilon}_c - (c_1/m)\dot{\varphi}_1 \qquad \ddot{\varphi}_2 = -P_2^2 \varphi_2 - (R/l_2)\ddot{\epsilon}_c - (c_2/m)\dot{\varphi}_2
\end{aligned}$$

Using the complex notation as before and solving

$$\varphi_1 = \left[\frac{N^2\omega^2(R/l_1)}{-N^2\omega^2 + P_1^2 + \iota N\omega(c_1/m)}\right]\epsilon_c$$

$$\varphi_2 = \left[\frac{N^2\omega^2(R/l_2)}{-N^2\omega^2 + P_2^2 + \iota N\omega(c_2/m)}\right]\epsilon_c$$

$$\epsilon_c = \frac{T_0/I_c}{\left[-N^2\omega^2 + S_3^2 - \dfrac{Q_1^2\left(P_1^2 + \iota N\omega \dfrac{c_1}{m}\right)N^2\omega^2 \dfrac{R}{l_1}}{-N^2\omega^2 + P_1^2 + \iota N\omega \dfrac{c_1}{m}} - \dfrac{Q_2^2\left(P_2^2 + \iota N\omega \dfrac{c_2}{m}\right)N^2\omega^2 \dfrac{R}{l_2}}{-N^2\omega^2 + P_2^2 + \iota N\omega \dfrac{c_2}{m}}\right]} \tag{24}$$

Now if both dampers are tuned to the disturbing frequency, $N^2\omega^2 = P_1^2 = P_2^2$. Substituting this and combining

$$\epsilon_c = \frac{T_0/I_c}{S_3^2 - N^2\omega^2[1 + (2mR^2/I_c)] + \iota N^2\omega^2 mR^2[(1/c_1) + (1/c_2)]} \tag{25}$$

Multiplying numerator and denominator by the conjugate of the denominator

$$\epsilon_c = \frac{T_0/I_c\{S_3^2 - N^2\omega^2[1 + (2mR^2/I_c)] - \iota N^2\omega^2 mR^2[(1/c_1) + (1/c_2)]\}}{\{S_3^2 - N^2\omega^2[1 + (2mR^2/I_c)]\}^2 + \{N^2\omega^2 mR^2[(1/c_1) + (1/c_2)]\}^2}$$

This can be checked for extreme values of $c_1$ and $c_2$. For $c_1 = c_2 = 0$, $\epsilon_c = 0$ as it should. For $c_1 = c_2 = \infty$

$$\epsilon_c = \frac{T_0/I_c}{S_3^2 - N^2\omega^2[1 + (2mR^2/I_c)]} = \frac{T_0}{K[1 - (N^2\omega^2/S_3'^2)]}$$

$S_3'$ is the natural frequency of the crankshaft vibrating with a node at the propeller but with the dampers clamped to the cheeks by the infinite $c_1$ and $c_2$.

The damper amplitudes will be

$$\varphi_1 = \left[\frac{N\omega(R/l)}{\iota(c_1/m)}\right]\epsilon_c \qquad \varphi_2 = \left[\frac{N\omega(R/l)}{\iota(c_2/m)}\right]\epsilon_c$$

The amplitude of each damper is a function of its own internal damping as well as $\epsilon_c$ so that for any given $\epsilon_c$

$$\varphi_1/\varphi_2 = c_2/c_1 \tag{26}$$

Thus, if $c_2 = c_1$, the two dampers will swing equal amounts. If $c_2 = c_1 = 0$, there is some ambiguity, since it would be theoretically possible for one damper to swing in a large enough amplitude to balance the disturbing torque, leaving the shaft at rest and no disturbance to excite the second damper. Another way of obtaining this condition would be to have $c_1$ equal zero and $c_2$ not equal zero. Then $\varphi_2$ would always be zero and the first damper would do all the "work." Actually $c_1$ and $c_2$ are never zero and both dampers will swing through amplitudes related according to Eq. (26).

It is clear from Eq. (25) that some crankshaft vibration will occur when $c_1$ and $c_2$ are greater than zero. Assume that $c_1 = c_2 = c$ and determine $\epsilon_c$ for an actual case. Then assume that $c_1 = c$ but that $c_2 = \infty$, giving a single damper, and calculate $\epsilon_c$ to see whether or not the addition of the second damper produces any beneficial effect.

The proper value for $c_1$ or $c_2$ is difficult to estimate. Theoretically, there is very little friction in the damper if it is considered that the damper swings with pure rolling motion occurring between the damper pins and the bushings. From the engine test, it appears, however, that there is considerable lateral vibration of the crankshaft which undoubtedly causes the damper to rub on the crankcheek, thus restraining the damper from swinging freely. The magnitude of this restraint will depend upon the pressure between the metal surfaces and the coefficient of friction. If the friction forces are those of dry friction, then the supposition of a damping coefficient proportional to the velocity will not be correct. If the friction forces are produced by the oil film between the damper and cheek surfaces, the supposition of damping proportional to the velocity would be more reasonable. The writer does not know which type of friction predominates and for simplicity has assumed that the damping is of a viscous nature in order to make the solution of the equations simple. As a means of evaluating the damping, let it be assumed that the maximum damping force is $f$ times the maximum restoring force, giving the following relationships: $cl\dot{\varphi}_{max.} = cl\varphi_1\omega(q/l)^{1/} = fm\omega^2 q\varphi_1$, from which $c = fm\omega(q/l)^{1/2}$, giving

$$N\omega^2 mR^2[(2/c)] = N^2\omega^2 mR^2\{[2/fm\omega(q/l)^{1/2}]\} = N\omega R^2(2/f) = (305 \times 10^2)(2/f)$$

Now considering Eq. (25) in the form for absolute values

$$|\epsilon_c| = \frac{T_0/I_c}{[\{S_3^2 - N^2\omega^2[1 + (2mR^2/I_c)]\}^2 + \{N^2\omega^2 mR^2[(1/c_1) + (1/c_2)]\}^2]^{1/2}}$$

For $c_1 = c_2 = c$

$$|\epsilon_c| = \frac{T_0/I_c}{10^6[0.542 + (0.00374/f^2)]^{1/2}}$$

Now for $T_0 = 10{,}000$ and $f = 0.05$: $|\epsilon_c| = 0.000545$ rad. or 0.031 deg.

For $c_2 = \infty$

$$|\epsilon_c| = \frac{T_0/I_c}{10^6[0.542 + (0.00374/f^2)(1/4)]^{1/2}} = 0.000815 \text{ rad. or } 0.047 \text{ deg.}$$

Comparing these last two solutions, it is seen that although the addition of the second damper reduces the crankshaft vibration the actual value of the vibration is somewhat independent of the damper factor $f$ just so long as this value is reasonably large. The reason for this is, of course, that even without the damper the crankshaft amplitude is not very great, because with the particular speed chosen the shaft is far from resonant. The first term of the denominator expresses the divergence from resonance of the system without the damper. If the crankshaft is operating near a critical speed for torsional vibration, this term will be very small or zero so that the last term expressing the effect of the damping becomes all important.

In the simplified system that has been used throughout this study, it is assumed that the propeller acts as a rigid flywheel and because of this only one resonant point for the system at approximately 1,200 r.p.m. was obtained. In actual practice, however, propeller blade flexibility may produce resonant points more dangerously placed in the operating range. However, for simplicity, consider Eq. (25) for the speed at which the first term in the denominator is zero. This corresponds to an engine r.p.m. of 1,175 and for this speed

$$\epsilon_c = \frac{T_0/I_c}{\iota N^2\omega^2 mR^2[(1/c_1) + (1/c_2)]}$$

For $c_1 = c_2 = c$

$$|\epsilon_c| = \frac{T_0/I_c}{N\omega R^2(2/f)}$$

For $c_1 = c$, $c_2 = \infty$

$$|\epsilon_c| = \frac{T_0/I_c}{N\omega R^2(1/f)}$$

From a comparison of these last two equations, it is apparent that the addition of a second damper, similar to the first, will reduce the shaft amplitude to one-half its former value when running at a resonant speed with some friction between the damper and the crankshaft.

## Single Damper Between Propeller and Crank Throw

It has been shown previously that a damper mounted on the rear crankcheek, i.e., antipropeller side of crank throw, should be tuned high to compensate for shaft flexibility. It will be of interest to determine what modifications are necessary in a damper mounted on the front crankcheek, i.e., between the propeller and the crankshaft, to compensate for the crankshaft flexibility. If in the system of Fig. 14 the rear damper is locked and it is assumed that the propeller is of finite size, since propeller vibration is of particular interest, the following equations of motion are obtained: for the propeller, $I_p\ddot{\alpha}_p = +K(\epsilon_2 - \alpha_p)$; for the front cheek, $I_c\ddot{\epsilon}_2 = -T_2(\epsilon_2 - \epsilon_c) + mR\omega^2 q\varphi_2 + c_2 l\dot{\varphi}_2 R - K(\epsilon_2 - \alpha_p)$; for the crankpin and rear cheek it will be assumed that $T_1$ is infinite, giving, $I_{cp}\ddot{\epsilon}_c = T_2(\epsilon_2 - \epsilon_c) + T_0 \sin N\omega t$; for the damper, $ml_2\ddot{\varphi}_2 = -m\omega^2 q\varphi_2 - mR\ddot{\epsilon}_2 - c_2 l_2\dot{\varphi}_2$. Solving these equations for the forced motion

$$\alpha_p = \frac{A}{E\left\{B - \dfrac{\dfrac{mR^2}{I_c}N^2\omega^2\left(P^2 + \iota N\omega\dfrac{c_2}{m}\right)}{-N^2\omega^2 + P^2 + \iota N\omega\dfrac{c_2}{m}}\right\} - C} \tag{27}$$

where

$$A = \frac{S_p^2 S_2^2 T_0}{I_{cp}(-N^2\omega^2 + S_{cp}^2)}$$

$$B = -N^2\omega^2 + S_2^2 + S_3^2 - \frac{S_2^2 S_{cp2}^2}{-N^2\omega^2 + S_{cp2}^2}$$

$$C = S_p^2 S_3^2$$

$$E = -N^2\omega^2 + S_p^2$$

Now, if there is no friction in the damper, $c_2 = 0$ and

$$\alpha_p = \frac{A}{E\left[B - \dfrac{(mR^2/I_c)N^2\omega^2 P^2}{-N^2\omega^2 + P^2}\right] - C}$$

From this expression it is evident that $\alpha_p$ will be zero when $P^2 = N^2\omega^2$. Therefore, if damper friction is negligible, the following conclusions are drawn for dampers mounted on the front crankcheek.

The damper should be tuned to the disturbing order so that it produces a node in the shaft at its attaching location. In tuning this damper the crankcheek flexibility from the damper pivot point to the crankshaft centerline should be considered and the damper tuned slightly high to compensate for this cheek flexibility. There is one possible difficulty with a damper installation of this type. Should there be a natural frequency mode of vibration which has one of its nodes at the front cheek, the damper will be ineffective in reducing vibration amplitudes for this mode. However, for a radial engine crankshaft any mode of this type would be of no importance for the following reasons:

(1) If the natural frequency were low (within the engine operating range), the disturbing force would be applied very near the node when compared to the location of the antinode, and even small friction damping forces acting on the shaft at the antinode where the amplitudes are large would effectively counteract a strong disturbance acting at a point where the amplitude is relatively small.

(2) If the mode of motion corresponds to an antinode at the crankpin, then, at resonance, dangerous amplitudes would be reached, but any mode of this type would have a frequency far above the operating range.

Now, if $c_2$ is not zero, it may be possible to adjust $P$ to obtain an $\alpha_p$ less than the value corresponding to $P = N\omega$. The general method here, would be to solve for the square of the magnitude of $\alpha_p$, differentiate the denominator with respect to $P$, and equate to zero in order to find the conditions for minimum $\alpha_p$.

This mode of attack, however, is unduly complex, so the mathematics is simplified by going back to Fig. 14, letting $T_1 = T_2 = .\infty$ and considering a single damper only. The equilibrium equations become

$$\ddot{\epsilon}_c = +Q^2P^2\varphi + (c_1/m)Q^2\dot{\varphi} - S_3^2\epsilon_c + (T_0/I_c)\sin N\omega t$$
$$\ddot{\varphi} = -P^2\varphi - (R/l)\ddot{\epsilon}_c - (c_1/m)\dot{\varphi}$$

Solving these equations

$$\varphi = \left[\frac{N^2\omega^2(R/l)}{-N^2\omega^2 + P^2 + \imath N\omega(c_1/m)}\right]\epsilon_c$$

$$\epsilon_c = \frac{T_0/I_c}{-N^2\omega^2 + S_3^2 - \dfrac{Q^2[P^2 + \imath N\omega(c_1/m)]N^2\omega^2(R/l)}{-N^2\omega^2 + P^2 + \imath N\omega(c_1/m)}}$$

Now, for the resonant speed $S_3^2 = N^2\omega^2$, and solving for the square of the magnitude of $\epsilon_c$

$$|\epsilon_c|^2 = \frac{(T_0/mR^2N^2\omega^2)^2}{\dfrac{[P^2(-N^2\omega^2 + P^2) + N^2\omega^2(c_1/m)^2]^2 + N^6\omega^6(c/m)^2}{[(-N^2\omega^2 + P^2)^2 + N^2\omega^2(c_1/m)^2]^2}}$$

Now, assume that there is some value of $P$ for which $|\epsilon_c|^2$ is a minimum, say, $P^2 = ZN^2\omega^2$; substituting this and considering the denominator only

$$\text{Denom.} = \frac{[ZN^2\omega^2(-N^2\omega^2 + ZN^2\omega^2) + N^2\omega^2(c/m)^2]^2 + N^6\omega^6(c/m)^2}{[(-N^2\omega^2 + N^2\omega^2Z)^2 + N^2\omega^2(c/m)^2]^2}$$

Now substituting $c/m = N\omega f$ and reducing

$$\text{Denom.} = \{[Z(Z-1) + f^2]^2 + f^2\}/\{[(Z-1)^2 + f^2]^2\}$$

Taking the derivative of this expression and equating to zero does not lead to a simple result. However, assume a value of $f$ and plot the expression to see how the function behaves.

Taking $f = 0.1$

$$\text{Denom.} = \{[Z(Z-1) + 0.01]^2 + 0.01\}/\{[(Z-1)^2 + 0.01]^2\}$$

In Fig. 15 the variation in the denominator as $Z$ changes is plotted. It is apparent that $Z$, slightly greater than one, gives the greatest denominator, and gives, therefore, the smallest $|\epsilon_c|$. For the curve shown, $f$ has been taken as 0.1. This is considered to be at least as large as, if not considerably larger than, the actual value ever experienced with a properly designed damper. It is interesting to note that as with shaft flexibility friction is partially compensated for by tuning high. However, the reduction in vibratory amplitude is very slight (approximately 1 per cent) and the change in tuning is also small—about 0.5 per cent. In a nine-cylinder radial engine the pendulum length would be shortened about 0.002 and, since this is of the same order of magnitude as the manufacturing tolerances on the parts, there is little hope of utilizing the "tuning to partially compensate for friction" refinement. Of course, it would be possible to reduce the tolerances, but the very slight gain in damper efficiency is hardly worth the increased manufacturing costs associated with very fine tolerances.

## Transient Conditions

In the previous analysis the forced motion only has been considered since our main interest has been the steady state. Our equations are good for all times except the very start of the vibration when the transient conditions become all important. The actual duration of the transient state is very short, and since tests indicate that there is nothing catastrophic about the transient conditions there is no grave mistake in neglecting them. However, it is of great academic interest and some practical importance to know just how the damper "builds up" its amplitude when the disturbing torque is suddenly applied. This is equivalent to spinning the crankshaft by external means, such as a windmilling propeller, and then turning on the ignition so that the firing frequency torque variation is suddenly applied.

In order to simplify the mathematics as much as possible, the two-mass system of Fig. 2 is considered, with the "windmilling speed" so far above resonance that the vibration torque of the propeller is negligible.

With a single damper on the crankcheek and with friction present the equations of motion are: for the crankcheek and the damper, respectively

$$\ddot{\epsilon} = (mRl/I)N^2\omega^2\varphi + (clR/I)\dot{\varphi} + (T_0/I)\cos(N\omega t + \delta)H(t) \tag{28}$$

$$\ddot{\varphi} = -N^2\omega^2\varphi - (R/l)\ddot{\epsilon} - (c/m)\dot{\varphi} \tag{29}$$

From Eq. (29) and using the operator notation

$$D^2\epsilon = -(l/R)[D^2 + (c/m)D + N^2\omega^2]\varphi$$

Substituting this in Eq. (28) and letting

$$\cos(N\omega t + \delta)H(t) = rp\,\epsilon^{\iota\delta}[1/(D - \iota N\omega)]\,D\,H(t)$$

where $rp$ stands for *real part of* and $H(t)$ is the heaviside unit function

$$\left[D^2 + \frac{c}{m}\left(1 + \frac{mR^2}{I}\right)D + N^2\omega^2\left(1 + \frac{mR^2}{I}\right)\right]\varphi = -\frac{T_0}{I}\,rp\,\frac{\epsilon_{\iota\delta}}{(D - \iota N\omega)}\,D\,H(t)$$

Equating the bracketed term on the left to zero and solving for $D$ the following roots are secured:

$$D = \frac{-\frac{c}{m}\left(1 + \frac{mR^2}{I}\right) \pm \left[\left(1 + \frac{mR^2}{I}\right)^2\left(\frac{c}{m}\right)^2 - 4\left(1 + \frac{mR^2}{I}\right)N^2\omega^2\right]^{1/2}}{2} = \alpha \pm \iota\beta \tag{30}$$

$$\varphi = -\frac{RT_0}{lI}\,rp\,\frac{\epsilon^{\iota\delta}}{[D - (\alpha + \iota\beta)]\,[D - (\alpha - \iota\beta)]\,[D - \iota N\omega]}\,D\,H(t)$$

Now, splitting this into partial fractions

$$\varphi = -\frac{R}{l}\frac{T_0}{I}\,rp\,\epsilon^{\iota\delta}\left[\frac{1}{[D - (\alpha + \iota\beta)]\,[+2\iota\beta]\,[\alpha + \iota(\beta - N\omega)]} + \frac{1}{[-\alpha + \iota(N\omega - \beta)]\,[-\alpha + \iota(N\omega + \beta)]\,[D - \iota N\omega]} + \frac{1}{[-2\iota\beta]\,[D - (\alpha - \iota\beta)]\,[\alpha - \iota(\beta + N\omega)]}\right]D\,H(t)$$

Performing the indicated operations

$$\varphi = -\frac{R}{l}\frac{T_0}{I}\,rp\left[\frac{1}{2\iota\beta[\alpha + \iota(\beta - N\omega)]}\,\epsilon^{(\alpha + \iota\beta)t + \iota\delta} - \frac{1}{2\iota\beta[\alpha - \iota(\beta + N\omega)]}\,\epsilon^{(\alpha - \iota\beta)t + \iota\delta} + \frac{1}{[\alpha^2 - \iota\alpha(N\omega + \beta) - \iota\alpha(N\omega - \beta) - (N^2\omega^2 - \beta^2)]}\,\epsilon^{\iota N\omega t + \iota\delta}\right]H(t)$$

Using the relation

$$\epsilon^{\iota(\beta t + \delta)} = \cos(\beta t + \delta) + \iota\sin(\beta t + \delta)$$

Simplifying and taking real parts

$$\varphi = -\frac{R}{l}\frac{T_0}{I}\left\{\frac{\epsilon^{\alpha t}}{2\beta}\left[\frac{\alpha\sin(\beta t + \delta) - (\beta - N\omega)\cos(\beta t + \delta)}{\alpha^2 + (\beta - N\omega)^2} - \frac{-\alpha\sin(\beta t - \delta) + (\beta + N\omega)\cos(\beta t - \delta)}{\alpha^2 + (\beta + N\omega)^2}\right] + \frac{(\alpha^2 + \beta^2 - N^2\omega^2)\cos(N\omega t + \delta) - 2\alpha N\omega\sin(N\omega t + \delta)}{\alpha^4 + N^4\omega^4 + \beta^4 + 2\alpha^2\beta^2 - 2N^2\omega^2\beta^2 + 2\alpha^2N^2\omega^2}\right\} \tag{31}$$

If $\delta = 0$ this equation reduces to

$$\varphi = -\frac{R}{l}\frac{T_0}{I}\,\frac{1}{[(\alpha^2 + \beta^2)^2 + N^2\omega^2(N^2\omega^2 + 2\alpha^2 - 2\beta^2)]}\left\{\epsilon^{\alpha t}\left[\frac{\alpha}{\beta}(\alpha^2 + \beta^2 + N^2\omega^2)\sin\beta t - (\alpha^2 + \beta^2 - N^2\omega^2)\cos\beta t\right] + (\alpha^2 + \beta^2 - N^2\omega^2)\cos N\omega t - 2\alpha N\omega\sin N\omega t\right\}$$

As before $c/m = N\omega f$, $\alpha = -(N\omega f/2)\,[1 + (mR^2/I)]$, $\beta^2 = (N^2\omega^2/4)\{[1 + (mR^2/I)]^2f^2 - 4[1 + (mR^2/I)]\}$, and $[1 + (mR^2/I)] = 1.128$; for $f = 0.05$, $N = 4.5$, $\alpha = -N\omega(0.0282)$, and $\beta = +N\omega(1.06)$.

Substituting these values

$$\varphi = -\frac{R}{l}\frac{T_0}{I}\frac{1}{0.02N^2\omega^2}\{\epsilon^{-0.0282N\omega t}[-0.0564\sin 1.06\,N\omega t - 0.121\cos 1.06\,N\omega t] + 0.121\cos N\omega t + 0.0564\sin N\omega t\}$$

For an engine speed of 2,000 r.p.m., $T_0 = 10{,}000$ in. lbs., $R = 5.677$, $I = 12.84$, and $l = 0.267$.

$$\varphi = -\{\epsilon^{-26.5t}[-0.0525\sin 1.06\,N\omega t - 0.113\cos 1.06\,N\omega t] + 0.113\cos N\omega t + 0.0525\sin N\omega t\} \tag{32}$$

The period of the damped free vibration is $T_n = [2\pi/1.06(941)] = 0.00630$ sec.
For the forced motion, $T_F = (2\pi/941) = 0.00667$ sec.

Theoretically, an infinite time is required for the steady state to be reached, but if the fact that the reduction of the free vibration to one-tenth its initial value constitutes the duration of the transient state is considered, then $\epsilon^{-26.5t} = 0.10$, from which $t = 0.087$ sec.

From this it is clear that the first term will be negligible after a very short time. Eq. (32) gives for the steady state

$$\varphi = -(0.113\cos N\omega t + 0.0525\sin N\omega t) \quad \varphi = -0.125\cos(N\omega t - 25°)$$

Check the direction of the damper swing as compared with the direction of the disturbing torque. At some value of $t$ which corresponds to an integral multiple of $2\pi$ for $N\omega t$, the torque $T_0\cos N\omega t$ will be maximum in the positive direction. The value of $\varphi$ will be negative, so that the torque exerted by the damper will be in the negative direction. This is as it should be if the damper torque is to balance the disturbing torque. For the case in question, where the friction in the damper is relatively large, the phase angle between the damper swing and the disturbing force is only 165 deg. instead of 180 deg. as it would be for a frictionless damper.

The amplitude of the damper torque will be given by

$$mR\omega^2 q\varphi \text{ max.} = [19.65(5.677)/386]\ [5.410]\ [2{,}000 \times (2\pi/60)]^2\ [0.125] = 8{,}560 \text{ in. lbs.}$$

As would be expected, this torque is slightly less than the disturbing torque. If the friction is reduced, the damper torque will approach the disturbing torque as a limiting value for a frictionless system.

In Fig. 16 the damper motion has been plotted from $t = 0$ to show the amplitude "build up." Note the very short time required for essentially steady state conditions to be reached.

It is rather paradoxical to note that for the transient condition that has been considered the crankshaft vibration is not reduced to zero because of the friction but that if this friction be eliminated crankshaft vibration is still present. This may be shown by substituting $c = 0$ in the previous equation and simplifying as follows:

$$\alpha = 0 \quad \beta = [(1 + mR^2/I)N^2\omega^2]^{1/2}$$

$$\varphi = -\frac{R}{l}\frac{T_0}{I}[1/(\beta^2 - N^2\omega^2)^2]\ [-(\beta^2 - N^2\omega^2)\cos\beta t + (\beta^2 - N^2\omega^2)\cos N\omega t]$$

From which

$$\varphi = \frac{(R/l)(T_0/I)}{[1 + (mR^2/I)]\,N^2\omega^2 - N^2\omega^2}[\cos\beta t - \cos N\omega t] = (T_0/mR\omega^2 q)(\cos\beta t - \cos N\omega t)$$

Since the damper torque is given by $T_D = mR\omega^2 q\varphi$, then $T_D = T_0(\cos\beta t - \cos N\omega t)$.

The last term in this equation represents a torque exerted on the crank masses by the damper, which is equal and opposite to the disturbing torque, thus preventing the disturbing torque from producing any vibration of the crank throw. The first term in the equation represents a torque numerically equal to the disturbing torque but at a frequency that corresponds to the natural frequency of the crank throw damper system. That $\beta$ corresponds to the natural frequency of the system may be shown as follows:

$$\beta = \left[\left(\frac{I + mR^2}{I}\right)\frac{q}{l}\omega^2\right]^{1/2}$$

but $\omega^2 q = (T_D/\varphi mR)$, giving

$$\beta = \left[\left(\frac{I + mR^2}{ImR^2}\right)\frac{T_D}{\varphi(l/R)}\right]^{1/2}$$

Noting that $\varphi(l/R)$ is the angular motion about the crankshaft axis of the damper relative to the crank throw and that $mR^2$ is the moment of inertia of the damper about the crankshaft axis, then

$$\frac{T_D}{\varphi(l/R)} = k_\theta = \text{the spring constant}$$

$I_D$ = moment of inertia of the damper, giving

$$\beta = \left[\left(\frac{I + I_D}{II_D}\right)k_\theta\right]^{1/2}$$

which is immediately recognized as the natural fre-

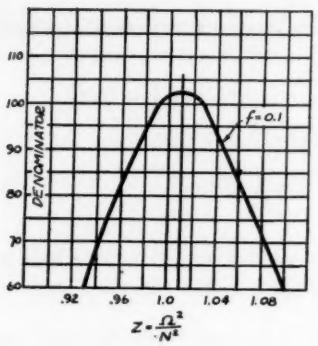


FIG. 15.

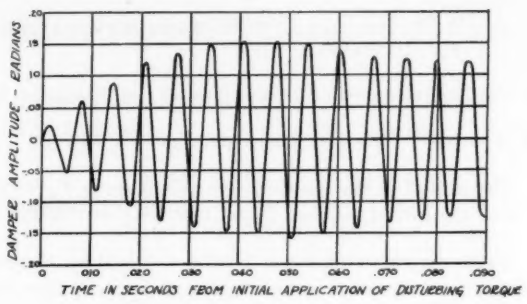


FIG. 16.

quency expression for the system. The free vibration is the source of the crankshaft amplitude which is produced when the damper is frictionless and the disturbing torque is suddenly applied.

The friction necessary to damp the transient condition is very small, however, and the most frictionless damper it is possible to build will still give the best vibration control.

## REFERENCES

[1] Taylor, E. S., *Eliminating Crankshaft Torsional Vibration in Radial Aircraft Engines*, S.A.E. Journal, March, 1936.

[2] Den Hartog, J. P., *Mechanical Vibrations*, First Edition, p. 97; McGraw Hill, New York, 1934.

[3] Taylor, E. S., Wright Aeronautical Corporation, Report No. 38, Project No. X-325, 1938.

[4] Timoshenko, S., *Applied Elasticity*, Westinghouse Technical Night School Press, Pittsburgh, 1927.

# Stress Analysis of Rings for Monocoque Fuselages

N. J. HOFF

*Polytechnic Institute of Brooklyn*

SUMMARY

Suggestions are made for reducing the work and for increasing the accuracy of the calculation of the unknown quantities in closed rings of arbitrary shape for monocoque fuselages. The advantages of assuming three or four imaginary pin-joints instead of an imaginary cut through the ring are shown. Graphic methods are introduced for the determination of the moment distribution in the "simple" system caused by the shear flow transmitted by the sheet covering. Worked out examples show the application of the principles to numerical problems.

## INTRODUCTION

THE CALCULATION of the moment distribution in closed rings for monocoque fuselages has a considerable literature. In all the papers that deal with the effect of the sheet covering of the fuselage the tacit assumption is made that the shear stresses transmitted from the ring to the covering can be calculated with sufficient accuracy from the formulas of Strength of Materials which are strictly valid only at some distance from the points of application of the loads. It is likely that this assumption is reasonable enough in the case of strong and stiff rings that transmit heavy loads. By this assumption the problem is reduced to the determination of the moments in a closed ring upon which a known system of self-equilibrating forces is acting.

A closed ring loaded in its own plane is three times statically indeterminate. It can be reduced to a "simple," or statically determinate structure by making a complete cut through it. The bending moment, the axial force, and the shear force acting in the imaginary cut are then the three "unknowns" which can be calculated by strain energy methods. Such a procedure is followed in Lundquist and Burke's paper[2] in which the unknowns are determined by Castigliano's theorem. With a view to taking advantage of the symmetry properties of the ring the cut is made at the topmost point of the ring and the origin of coordinates is assumed to be at the same point. Their paper also contains references to earlier literature. Of the more recent publications, Ruffner's[4] and Wise's[5] papers deal with circular rings and make use of the same system of unknowns, while Liepmann[1] follows Müller-Breslau's lead in assuming the unknown quantities to act at the "elastic center" of the ring.

The above choices of the unknowns, as a rule, result in obtaining the resultant moments in the indeterminate structure as small differences of large quantities. Indeed, Ruffner suggests carrying out all calculations to five significant figures in order to be sufficiently accurate. This requirement may lead to great difficulties in cases where the shape of the ring is not known analytically.

In the present paper suggestions are made for a more convenient choice of the unknowns. Moreover, the use of graphic methods is shown for the calculation of the bending moments in the "simple" structure. It is believed that the procedure outlined is of advantage in the calculation of rings the shape of which cannot be expressed by simple analytic formulas. Throughout the paper it is assumed that Hooke's law is valid, that the strain energy due to axial and to shear forces can be neglected, and that the direct stress distribution over the cross-section due to bending is linear. Bending moments are considered positive if they cause tension on the outside of the ring.

## GRAPHIC METHODS

Fig. 1a shows the graphic determination of the bending moment that acts in a section $x$–$x$ of a curved beam pinned at its ends at 1 and 2. The full line represents the center line of the beam; the dotted line, the center line of the thin sheet covering attached to the ring. It is known that if a constant clockwise shear flow $s$ lbs./in. is transmitted from the covering to the ring and the figure was originally drawn to $^1/_{10}$ scale, the moment $M_s$ with respect to section $x$ of the total shear flow extending from 1 to $x$ is $M_s = 2 \times 10^2 s A_s$, where $A_s$ is the obliquely shaded area measured in sq.in. and $M_s$ is given in in. lbs. If, simultaneously, a concentrated load is also acting—as the reaction $R_1$ in Fig. 1a—it is convenient to represent it by a vector of the length $R_1/10s$. Its moment $M_R$ with respect to section $x$ is $M_R = -2 \times 10^2 s A_R$, where $A_R$ is the horizontally shaded area and the negative sign indicates a counterclockwise moment.

Consequently, the resultant moment at $x$ can be obtained by planimetering the difference of the two areas. This can be done quickly, for a number of sections and the moment diagram over the curved bar can easily be drawn.

In the case of a variable shear flow the same procedure can be followed after a "reduced" moment area has been constructed. In Fig. 1b, originally drawn to $^1/_5$ scale, the shear flow varies from $s_1$ at point 1 to $s_2$ at

Presented at the Structures (Part 1) session, Tenth Annual Meeting, I.Ae.S., New York, January 28, 1942.

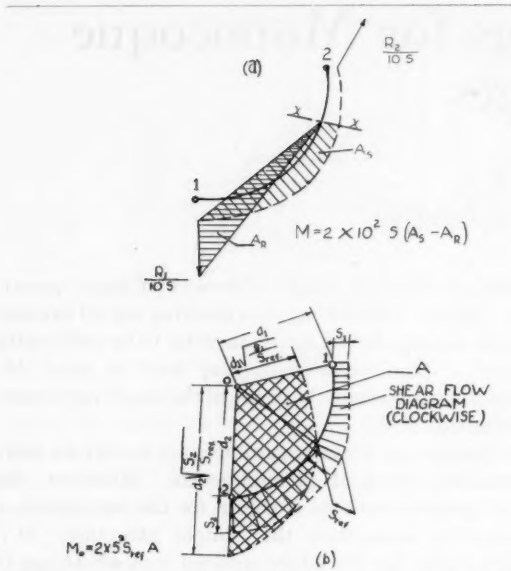


FIG. 1. a. Constant shear flow. b. Variable shear flow.

point 2. An intermediate value is chosen for the "reference shear" $s_{ref.}$, and the square root of the ratio $s/s_{ref.}$ is calculated at a number of sections. The moment $M_0$ of the variable shear flow in the sheet 1–2 with respect to point $O$ is $M_0 = 2 \times 5^2 s_{ref.} A$, where $A$ is the cross-hatched reduced moment area obtained by multiplying the distance of the shear flow from point $O$ by the square root of the respective shear ratio.

If all drawings are made to the same scale and a reference shear is chosen, it is convenient to think of the forces in terms of lengths and of the moments in terms of areas. A conversion into lbs. and in. lbs. may be made before or after the strain energy calculations by multiplying (1) forces by the reference shear flow and by the reciprocal of the scale and (2) moments by the reference shear flow and by the reciprocal of the square of the scale.

## THE BEST CHOICE OF THE UNKNOWNS

When deciding upon the best choice of the unknown quantities, one should consider the following three main requirements: (1) the computational work should be small; (2) the accuracy should be great; and (3) the moments in the simple structure should differ as little as possible from those in the complete structure.

Fulfillment of the third requirement, as a rule, includes the fulfillment of the first two. The calculation of the unknowns assumes the character of a correction of the values of the moments in the simple structure if these are not far from the actual moments in the complete structure. For instance, if the difference between the final moments and those in the simple structure amounts to 10 per cent, then an error of 10 per cent in the value of the unknowns causes an error of only 1 per cent in the final moments. On the other hand, if the final moments in the complete structure are obtained as small differences of the moments in the simple structure due to the external loads and those caused by the unknowns, then an error of 1 per cent in the value of the unknowns may cause in actual cases an error of 20–30 per cent in the value of the final moments in the complete structure. Furthermore, compliance with the third requirement allows a good preliminary proportioning, which is of importance when the ring is of variable cross-section.

The choice of the unknowns in all the papers cited is such that the moments caused by the external loads in the simple system differ a great deal from the moments in the complete system. This results in the necessity of computations to five digits as suggested by Ruffner. Such a procedure can be avoided if, instead of making a complete cut through it, imaginary pin-joints are inserted into the ring. Three imaginary joints transform the statically indeterminate closed ring into a simple (determinate) structure. The three unknowns are then the three bending moments that in reality are acting in the sections where the imaginary joints are inserted.

With a good power of visualizing distortions, based on experience in calculation and experiment, the aircraft stress analyst should be able to predict approximately the inflection points in the distorted shape of the ring under a given system of loads. If the imaginary joints were inserted at the actual inflection points, the unknown moments would vanish. Hence, with a good guess for the location of the joints the unknowns must be small.

According to Castigliano's theorem, the unknown moments make the strain energy stored in the ring a minimum. Therefore, the differential coefficients of the strain energy with respect to the unknown moments $X_m$, $X_p$, and $X_v$ at the imaginary joints $m$, $p$, and $v$, respectively, must vanish. These requirements lead to equations identical with Eqs. (8) in Lundquist and Burke's paper if $M_m$, $M_p$, and $M_v$ denote the bending moments at any section of the ring caused by a unit moment applied at the $m$th, $p$th, and $v$th imaginary joint, respectively. $M_0$ is the bending moment at any section of the ring caused by the external loads in the simple system; $E$, the modulus of elasticity; $I$, the moment of inertia of the section; and $ds$, the element of length of the center line of the ring. The first of Eqs. (8) in Lundquist and Burke's paper is

$$X_m \int \frac{M_m^2}{EI}\,ds + X_p \int \frac{M_m M_p}{EI}\,ds + X_v \int \frac{M_m M_v}{EI}\,ds + \int \frac{M_m M_0}{EI}\,ds = 0$$

The three equations can also be written in the form

$$\begin{aligned} X_m\delta_{mm} + X_p\delta_{mp} + X_v\delta_{mv} + \delta_{m_0} &= 0 \\ X_m\delta_{pm} + X_p\delta_{pp} + X_v\delta_{pv} + \delta_{p_0} &= 0 \\ X_m\delta_{vm} + X_p\delta_{vp} + X_v\delta_{vv} + \delta_{v_0} &= 0 \end{aligned} \qquad (1)$$

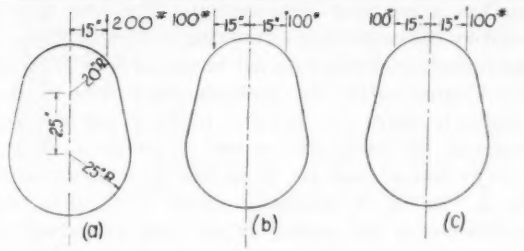


FIG. 2. External loads.

where

$$\delta_{jk} = \int (M_j M_k / EI)/ds \qquad (1a)$$

In the case of a ring of arbitrary shape the integrals indicated in Eq. (1a), as a rule, must be computed graphically. In the graphic integration the effect of a variable moment of inertia can easily be taken into account. Solving Eqs. (1), one obtains the values of the unknown moments that act at the imaginary joints.

The above is the procedure to be followed when the ring is not symmetric. If symmetric or antisymmetric loads act upon a symmetric ring, the calculations are materially simplified. In many cases it is advantageous to resolve nonsymmetric loads into symmetric and antisymmetric groups of loads, as discussed in a recent paper published by Newell.[3] This can be done as shown in Fig. 2, where load (a) is equivalent to the simultaneous action of loads (b) and (c). In such a case, however, little is gained if the bending moments caused by the unknowns are nonsymmetric. To remedy this situation it is suggested that the unknowns also be combined into symmetric and antisymmetric groups.

In Fig. 3 the three imaginary joints are located at points $A$, $B$, and $C$, respectively. The three unknown moments are denoted $M_A$, $M_B$, and $M_C$, respectively. The combination $M_A = M_B = M_C = 1$ is symmetric and causes a uniform bending moment distribution over the ring. In the following calculations this group of unknowns is called group $m$ and the corresponding bending moments are denoted $B_m$. The symmetric group $p$ consists of the simultaneously acting moments $M_A = 1$ and $M_B = 1$. The bending moment diagram $B_p$ is the same as that caused by a (horizontal) tension at $C$ of a magnitude equal to unity divided by the vertical distance from $A$ to $C$. This follows from the moment equilibrium of the curved bar $A$–$B$ and from the symmetry condition that the reaction at joint $C$ must be horizontal. Finally, the antisymmetric group $v$ is formed by the moments $M_A = -1$ and $M_B = 1$. The corresponding bending moment diagram $B_v$ is the same as that caused by a (vertical) shearing force at $C$ of a magnitude equal to unity divided by the horizontal distance from $A$ to $C$. This follows again from the moment equilibrium of bar $A$–$B$ and from the antisymmetry condition that the reaction at $C$ must be vertical.

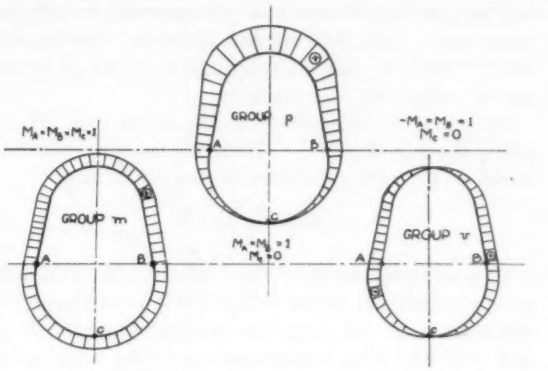


FIG. 3. Groups of moments.

It is easy to prove that the differential coefficients of the strain energy with respect to the groups $m$, $p$, and $v$ vanish. It was stated before that if the unknown bending moments at the imaginary joints are denoted $M_A$, $M_B$ and $M_C$, respectively, and the symbol

$$U = f(M_A, M_B, M_C) \qquad (2)$$

is used for the strain energy then by Castigliano's theorem

$$\frac{\partial U}{\partial M_A} = 0 \qquad \frac{\partial U}{\partial M_B} = 0 \qquad \frac{\partial U}{\partial M_C} = 0 \qquad (3)$$

If three groups of moments $X_m$, $X_p$, and $X_v$ are formed by three independent linear combinations, such that

$$\begin{aligned} X_m &= a_1 M_A + b_1 M_B + c_1 M_C \\ X_p &= a_2 M_A + b_2 M_B + c_2 M_C \\ X_v &= a_3 M_A + b_3 M_B + c_3 M_C \end{aligned} \qquad (4)$$

where $a_1, a_2, \ldots c_3$ are arbitrary constants, Eq. (2) can be written in the form

$$U = F(X_m, X_p, X_v) \qquad (5)$$

Differentiating with respect to $M_A$, one obtains

$$\frac{\partial U}{\partial M_A} = \frac{\partial U}{\partial X_m}\frac{\partial X_m}{\partial M_A} + \frac{\partial U}{\partial X_p}\frac{\partial X_p}{\partial M_A} + \frac{\partial U}{\partial X_v}\frac{\partial X_v}{\partial M_A} = 0 \qquad (6)$$

Two similar equations are obtained if one differentiates with respect to $M_B$ and $M_C$. If the partial differential coefficients $\partial X_m/\partial M_A$, $\partial X_m/\partial M_B$, . . . $\partial X_v/M_C$ are calculated from Eqs. (4) and substituted into the three equations the first of which is Eq. (6), the following system of simultaneous equations is obtained:

$$\begin{aligned} a_1(\partial U/\partial X_m) + a_2(\partial U/\partial X_p) + a_3(\partial U/\partial X_v) &= 0 \\ b_1(\partial U/\partial X_m) + b_2(\partial U/\partial X_p) + b_3(\partial U/\partial X_v) &= 0 \\ c_1(\partial U/\partial X_m) + c_2(\partial U/\partial X_p) + c_3(\partial U/\partial X_v) &= 0 \end{aligned} \qquad (7)$$

The unique solution of this system of homogeneous linear equations is:

$$\partial U/\partial X_m = 0 \quad \partial U/\partial X_p = 0 \quad \partial U/\partial X_v = 0 \qquad (8)$$

as long as the denominator determinant is different from zero. The determinant, however, can be zero only if Eqs. (4) are interdependent, which is incompatible with the assumptions.

Carrying out the operations indicated in Eqs. (8), one again obtains Eqs. (1). With the present notation, however, Eq. (1a) should be written in the form

$$\delta_{jk} = \int (B_j B_k / EI)\, ds \tag{9}$$

This result means that when one determines the integrals symbolically given in Eq. (9) it is permissible to introduce into the ring the imaginary joints $A$, $B$, and $C$ of Fig. 3 for the calculation of the bending moments caused by the external loads and at the same time to use the bending moments caused by the unknown moment, the unknown direct force, and the unknown shear force which act in a complete cut through the ring at $C$.

In some cases like that of the second numerical example, two inflection points appear on either side of the axis of symmetry of the ring, and both inflection points are at a considerable distance from the axis of symmetry. In such a case the assumption of an imaginary joint at point $C$ is too remote from reality. Full advantage can be taken of the properties of symmetry only if four imaginary pin-joints are introduced into the ring. This, however, makes the system movable. The second example shows how equilibrium under the given external loads can be established in such a movable system. It is suggested to make use again of the groups of unknowns shown in Fig. 3 and to calculate $X_m$, $X_p$, and $X_v$ from Eqs. (1) and (9). This is permissible, since the bending moment distribution due to the external loads in the movable system can be transformed into a moment distribution in a ring completely cut at $C$ by superimposing the moments $B_m$, $B_p$, and $B_v$ multiplied by suitable constant factors. These factors must be so chosen that after the superposition the bending moment, the direct force, and the shear force in the section at $C$ should vanish. If, however, $B_0$ in the movable system is just a linear combination of $B_0$ in the completely cut system and of $B_m$, $B_p$, and $B_v$, then Eqs. (1) and (9) determine the values of $X_m$, $X_p$, and $X_v$ which make the strain energy a minimum.

It follows from Eqs. (1) and (1a) (or (9)) that in the case of symmetric rings all coefficients $\delta_{jk}$ vanish in whichever one of the two moments $M_j$, $M_k$ (or $B_j$, $B_k$) is symmetric and the other antisymmetric. Also, it is allowable to calculate all the nonvanishing coefficients for one-half of the ring.

## Torsion

The first numerical example calculated here is shown in Fig. 2b. For the sake of simplicity it is assumed that the distance between the sheet covering and the center line of the ring is negligibly small and that the ring has a constant cross-section. The area $A$ enclosed by the center line of the ring is $A = 2752$ sq.in. The counterclockwise external torque is $T = 3000$ in. lbs. Consequently, the uniform shear flow in the covering becomes $s = T/2A = 0.544$ lb. per in. The imaginary pin-joints are assumed at points $A$, $B$, and $C$. The former two are 30 in. above $C$ as shown in Fig. 3. In Fig. 4, originally drawn to $^1/_{10}$ scale, the equilibrium of the portion of the ring extending between the joints at $B$ and $C$ is established. The area between the straight line $BC$ and the arc $BC$ was 2.6 sq.in. Hence, the moment with respect to $B$ of the uniform shear flow between $B$ and $C$ was $2A = 5.2$ sq.in. Since the loading (torque) is antisymmetric, the reaction at $C$ cannot have a horizontal component. Therefore, the (vertical) reaction at $C$ was $R_C = 2.12$ in., since the horizontal distance from $B$ to $C$ was 2.46 in. in the drawing. The resultant of the shear flow has a length equal to the distance $B$–$C$ (3.87 in.) and is parallel to $B$–$C$. Consequently, the reaction at $B$ had the length 5.67 in. as shown in the figure, since for reasons of equilibrium the three forces must form a closed polygon. The equilibrium of moments is also satisfied, since in reality the line of action of $R_R$ passes through the intersection point of $R_B$ and $R_C$.

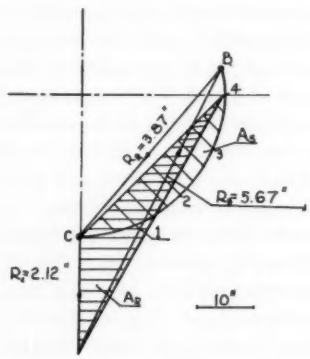


Fig. 4. Equilibrium of lower part (torsion).

The bending moment at station 4 is $(A_S - A_R)$ sq.in. In the same way the bending moments at stations 1–3 may be found with the aid of a planimeter. The bending moments in the upper part of the ring can be similarly determined from the uniform shear flow and from the reaction $-R_B$. In Fig. 5 the moments $B_0$ so obtained are plotted against the developed length of one-half of the ring. Curve $B_v$ is also plotted and is magnified sixfold for the sake of a convenient representation.

Since the external load is antisymmetric, the coefficients $\delta_{m0}$ and $\delta_{p0}$ defined by Eq. (9) must vanish. Hence, the unique solution of the first two of Eqs. (1) is $X_m = X_p = 0$. In the third equation the symmetric-antisymmetric combinations $\delta_{vm}$ and $\delta_{vp}$ must vanish. The remaining two coefficients

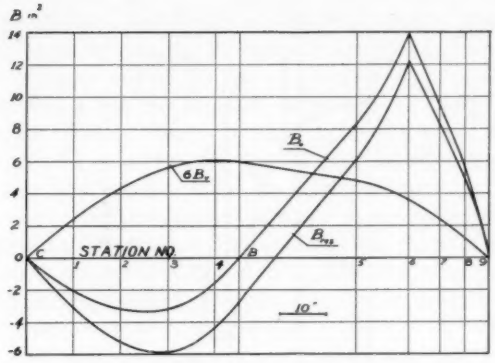


FIG. 5. Bending moments due to torsion.

$$EI\delta_{vv} = \int B_v^2\, ds$$

and

$$EI\delta_{v_0} = \int B_v B_0\, ds$$

are the areas below the $B_v^2$, and the $B_0 B_v$ curve, respectively, shown in Fig. 6. Since the developed length of the ring was also originally drawn to $^1/_{10}$ scale, the planimetered areas had the values 5.30 in.$^5$ and 14.55 in.$^5$, respectively. A conversion into in.$^3$ lbs.$^2$ is not necessary, and after the common factor $EI$ is cancelled the third of Eqs. (1) becomes $15.55 + 5.30\, X_v = 0$ or $X_v = -2.75$. The resultant moment curve in the complete structure has the ordinates $B_0 - 2.75\, B_v$ and is denoted $B_{res.}$ in Fig. 5.

It is seen that the guess for the location of the inflection point was a good one, and the final moments $B_{res.}$ differ but little from those represented by the $B_0$ curve. The conversion factor is $0.544 \times (10^2)$. Consequently, the greatest positive moment is $M = 666$ in. lbs., and the greatest negative moment is $M = -319$ in. lbs.

## BENDING

The second numerical example is shown in Fig. 2c. For the sake of simplicity it is assumed that the fuselage is a single shell of a (fully effective) wall thickness $t$. A numerical calculation gives $I/t = 55{,}000$ cu.in. for one-half of the fuselage section. The shear flow $s$ in a section $x$ is calculated by the known formula $s = (S/I)F$, where $S = 100$ lbs. is the total shear force; $I$, the moment of inertia; and $F$, the first moment of the portion beyond the section $x$ of the cross-section of the fuselage. Consequently, $s = (100/55{,}000)\,(F/t)$.

As a reference shear flow $s_{ref.} = s^*$, the total shear force divided by the total length $L = 96.2$ in. of one-half of the circumference of the fuselage is taken arbitrarily: $s^* = s_{ref.} = 1.04$ lbs. per in. Hence, the shear ratio is $s/s_{ref.} = 1.75 \times 10^{-3}\, F/t$. Fig. 7 shows the shear flow distribution. For convenience the values of the shear ratio and of its square root are noted at 14 stations.

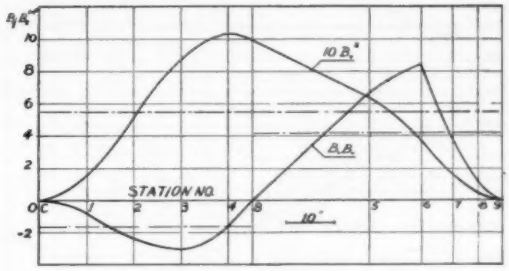


FIG. 6. Graphical integration (torsion)

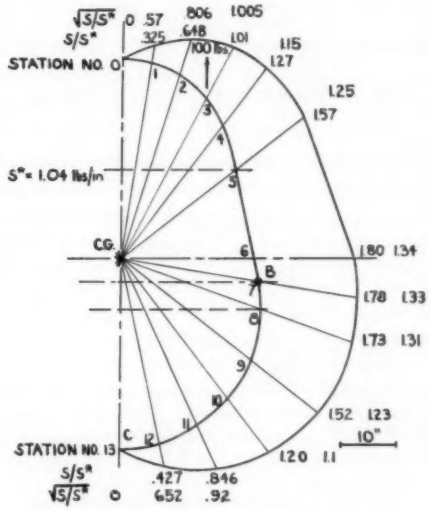


FIG. 7. Shear distribution in bending

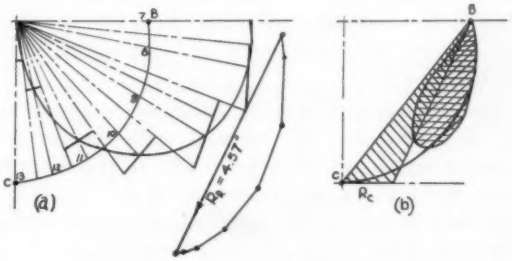


FIG. 8. a. Resultant of shear flow (bending). b. Equilibrium of lower part (bending).

For a trial the same three imaginary joints are assumed as in the case of torsion and the unknowns are again combined into the groups shown in Fig. 3. In Fig. 8 the equilibrium of the lower part of the ring is established. The resultant of the variable shear flow is constructed in Fig. 8a by adding up vectorially the stretches between consecutive stations representing shear forces, after multiplying them by the corresponding shear ratio. In Fig. 8b the cross-hatched area is one-half of the moment with respect to $B$ of the variable shear flow from $B$ to $C$. It is constructed by multiplying the distances from point $B$ to points on the

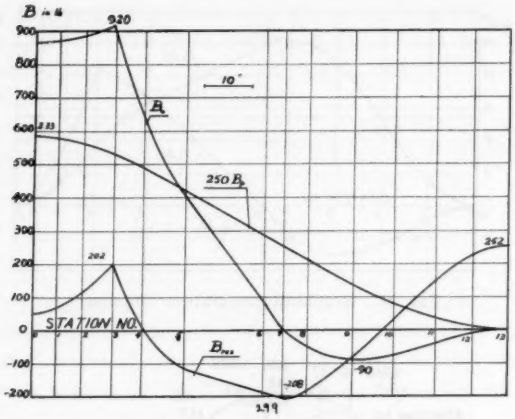


FIG. 9. Bending moments due to bending.

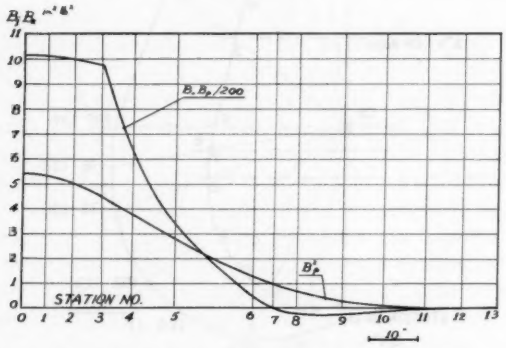


FIG. 10. Graphical integration (bending).

arc $B$–$C$ by the square root of the shear ratio, as explained in connection with Fig. 1. (The drawing is not correct, the curve ought to be tangential to the straight line $B$–$C$.)

The reaction at $C$ must be horizontal since the loading is symmetric. Its moment with respect to $B$ must be equal and opposite to that of the shear flow since there is an imaginary pin at $B$. In Fig. 8*b*, originally drawn to $^1/_{10}$ scale, the cross-hatched area was 1.43 sq.in. Hence, the reaction at $C$, $R_C = 0.95$ in., since the vertical distance from $B$ to $C$ was 3 in. The moments are easily determined with a planimeter after the reduced moment areas have been constructed for different sections of the ring. The reaction at $B$ can be constructed graphically since $R_B$ and $R_C$ are known.

Fig. 9 contains the converted moment curves $B_0$ and $B_p$. The conversion factor is $1.04 \times 10^2$. The curve $B_m = 1$ is not shown, since it would be just a straight horizontal line. The area below the $B_0$ curve is consequently equal to $\int B_m B_0\, ds$; that below the $B_p$ curve is equal to $\int B_m B_p\, ds$. The remaining two non-vanishing integrals are determined by planimetering the areas below the curves shown in Fig. 10. Altogether the following values were obtained:

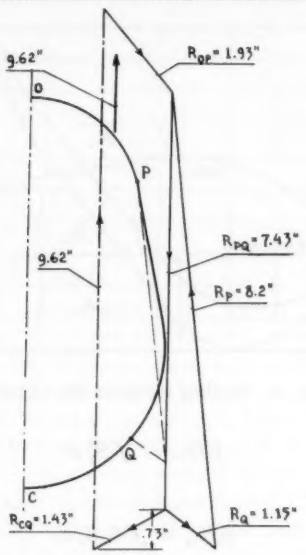


FIG. 11. Equilibrium in movable system.

$$\int B_0 B_m\, ds = 25{,}600 \text{ in.}^3 \text{ lbs.}^2$$
$$\int B_0 B_p\, ds = 55{,}800 \text{ in.}^3 \text{ lbs.}^2$$
$$\int B_m^2\, ds = 96.4 \text{ in.}^3 \text{ lbs.}^2$$
$$\int B_p^2\, ds = 181.7 \text{ in.}^3 \text{ lbs.}^2$$
$$\int B_m B_p\, ds = 109.0 \text{ in.}^3 \text{ lbs.}^2$$

Consequently, the solution of Eqs. (1) is

$$X_m = 252 \qquad X_p = -460 \qquad X_v = 0$$

The resultant moment is

$$B_{res.} = B_0 + 252 B_m - 460 B_v$$

It is plotted in Fig. 9. It is seen that the resultant moment is the difference of large quantities and differs considerably from the moments $B_0$ in the simple structure. This is contrary to the third requirement for the best choice of the unknowns.

It is possible to get a better agreement between the $B_0$ and $B_{res.}$ curves if $B_0$ is calculated for a movable system obtained by the introduction of four imaginary joints. If an equilibrium with the external loads can be established in this movable system, by Castigliano's theorem the actual moment distribution can be found as that combination of the so-obtained $B_0$ moment diagram with the $B_m$, $B_p$, and $B_v$ moment diagrams of Fig. 3 that corresponds to the least strain energy.

The movable system is shown in Fig. 11. $R_{PQ}$ is the resultant shear force acting on the portion of the ring extending from point $P$ to point $Q$. Its magnitude, direction, and line of action have been determined by making use of the reduced moment areas, as explained before. The magnitude and direction of the resultant shear force acting on parts $O$–$P$ and $C$–$Q$ have been similarly determined. The three form a closed polygon with the vertical external force 100 lbs. = 9.62 in.

The moment equilibrium of part $P$–$Q$ requires that the reactions $R_P$ and $R_Q$ at points $P$ and $Q$, respectively, should intersect on the line of action of $R_{PQ}$. This requirement can be satisfied in an infinite number of ways. Since, however, no shear force may act at $O$ because of symmetry, the vertical component of the reaction at $P$ must balance the resultant of 9.62 in. and of the vertical component of $R_{OP}$. A similar condition exists for the vertical component of the reaction at $Q$. Hence, the ratio of the vertical distances of points $P$ and $Q$, respectively, from the intersection point of the two reactions with $R_{PQ}$ is $(R_P)_v/(R_Q)_v = 8.16/0.73$.

This requirement determines the location of the intersection point and, consequently, the directions of the reactions. These being known, the magnitudes of the reactions follow from the graphic construction shown in Fig. 11. The equilibrium of part $O$–$P$ is established if the necessary horizontal reaction and bending moment are assumed to act at point $O$. This is permissible, since by symmetry an equal and opposite moment and horizontal force are required for the equilibrium of the other (not shown) half of the ring. Similar considerations hold true for part $C$–$Q$.

From this point the procedure is the same as before. Fig. 12 shows the curves $B_0$ and $B_0B_p/2$. The area below these curves was determined with a planimeter and was 2.17 and 2.89 sq.in., respectively. Hence,

$$\int B_0 B_m \, ds = 2250 \text{ in.}^3 \text{ lbs.}^2$$

$$\int B_0 B_p \, ds = 6000 \text{ in.}^3 \text{ lbs.}^2$$

The remaining integrals retain the values calculated for the first choice of the imaginary joints. Consequently, the solution of Eqs. (1) is

$$X_m = 43.7 \qquad X_p = -59 \qquad X_v = 0$$

The resultant moment $B_{res.}$ is shown by a full line in Fig. 12. It differs little from $B_0$.

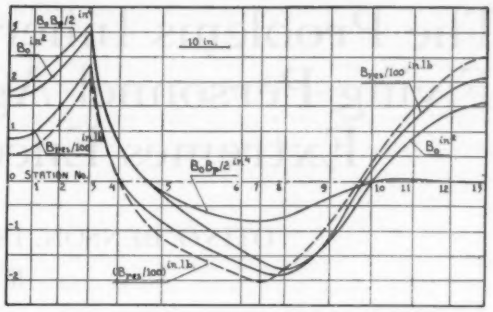


FIG. 12. Final moments in bending.

For the sake of comparison the $B_{res.}$ curve calculated on the first assumption for the imaginary joints is replotted in Fig. 12 and shown by the dotted line. Its agreement with the full line can be considered good if one takes into account that the first choice of the imaginary joints was poor, that the numerical calculations were carried out on the slide rule, and that the graphic constructions were made on $8\frac{1}{2}$ by 11 in. sheets of paper.

## REFERENCES

[1] Liepmann, Hans P., *General Stress Analysis for Rings with One Axis of Symmetry*, Journal of the Aeronautical Sciences, Vol. 7, No. 12, p. 509, October, 1940.

[2] Lundquist, E. E., and Burke, W. F., *General Equations for the Stress Analysis of Rings*, N.A.C.A. T.R. No. 509, 1934.

[3] Newell, J. S., *The Use of Symmetric and Anti-Symmetric Loadings*, Journal of the Aeronautical Sciences, Vol. 6, No. 6, p. 235, April, 1939.

[4] Ruffner, B. F., Jr., *Monocoque Fuselage Circular Ring Analysis*, Journal of the Aeronautical Sciences, Vol. 6, No. 3, p. 114, January, 1939.

[5] Wise, J. A., *Analysis of Circular Rings for Monocoque Fuselages*, Journal of the Aeronautical Sciences, Vol. 6, No. 11, p. 460, September, 1939.

# The Problems Inherent in the Protection of Flying Personnel Against the Temperature Extremes Encountered in Flight

OTIS O. BENSON, JR., AND ERNEST A. PINSON*
*Wright Field*

THE HUMAN BODY of its own volition always and usually quite unconsciously perspires, exercises, shivers and even puts on clothing with one aim in mind—that is, to always balance its heat loss with its heat production so that the internal body temperature is maintained at 98.6°F. (37°C). To protect against excessive heat, the microthermostat that controls the temperature regulation of the body causes sweating, which under conditions of comfort should be avoided. To protect against cold this same microthermostat causes stasis of the blood in the peripheral layers of skin (vasoconstriction) and can even stimulate shivering. For proper protection against cold, however, the body uses clothing for heat insulation.

The problem of maintaining heat balance in the flyer is unusual in two main respects. First, with respect to the extremely low environmental temperatures which are encountered in flight, and secondly, with respect to the rapidly changing environmental conditions as changes in altitude are effected. On the average, in this latitude, there is a temperature decrease of about 3.5°F. with each 1,000-ft. increase in altitude until a temperature of −67°F. (−55°C.) is reached. The temperature decline with increasing altitude apparently ceases when a temperature of −70°F. is attained. In going from sea level to 30,000 ft., an aviator will encounter a temperature drop of approximately 105°F. (3.5°F. × 30), that is, he may go from a temperature of 70°F. on the ground to a temperature of −35°F. at 30,000 feet. Suitable clothing at one of these temperatures will obviously not be suitable at the other. This poses a particularly difficult problem for the pursuit pilot, or any other member of an airplane crew, who cannot easily put on or take off clothing while in flight.

The solution to the problem of maintaining heat balance in flying personnel under such rapidly changing environmental conditions, and at the extremely low temperatures encountered at high altitudes, has progressed along three rather logical and distinct pathways. Each mode of solution will be discussed together with its individual merits and its objectionable features. This will be followed by an analysis of the future possibilities of each of the various trends in relation to the final solution of the problem.

Presented at the Physiologic Problems session, Tenth Annual Meeting, I.Ae.S., New York, January 29, 1942.

*U.S. Army Medical Research Unit, Equipment Laboratory, Experimental Engineering Section, Materiel Division.

## FIRST SOLUTION

One of the solutions involves heating of the cabin of the plane to a temperature at which the occupants can maintain heat balance and be comfortable when wearing ordinary clothing.

### *Advantages*

(a) The advantages of this system lie in the fact that the heat supplied can be adjusted as outside conditions change, and in that the activities of the personnel are not restricted by heavy clothing.

### *Disadvantages*

(a) No protection is afforded against cold in case of failure of the heating system or in the event of forced landing and abandonment of ship on a cold terrain.

(b) Condensation of moisture or frost on window surfaces hampers visibility. It has been proved by experience that this is particularly undesirable and dangerous, especially on high altitude bombing and combat missions.

(c) Low heat capacity of rarefied air at 30,000 or 35,000 ft. seriously reduces the efficiency of this method of warming the plane.

In order for this mode of maintaining body heat balance to be effective, the interior walls of the crew compartment must be kept warm enough so that heat loss by radiation from the body to the walls does not become too large. Whether or not enough heat can be absorbed by the walls from the heated air inside the plane in the cold rarefied atmosphere of high altitudes is probably dependent chiefly upon the insulation afforded by the thickness and substance of the plane wall itself. The maintenance of the interior of a thin metal fuselaged plane at an acceptable radiation temperature may be difficult. The development of pressure cabin planes with the consequent increase in cabin wall thickness, and also increase in the specific heat of air inside the plane as compared with that of the less dense air outside, will improve conditions for this mode of solution.

Heat derived from compression of air for the pressure cabin is utilized in warming the cabin air, thus permitting elimination of a certain weight of heating equipment as such.

The future possibilities of this solution to the problem will certainly be enhanced by development of the pressure cabin plane. If the window frosting problem can then be solved, this solution to the problem of body heat balance may develop into a satisfactory one.

### Second Solution

The second solution to the problem involves the use of sufficient unheated insulated clothing to enable each crew member to reduce heat loss sufficiently to maintain heat balance.

#### *Advantages*

(a) The main advantage of this solution lies in the independence of each crew member of outside sources of heat under all conditions, including forced landing and abandonment of ship on a cold terrain.

#### *Disadvantages*

(a) Inability to adjust the amount of clothing to suit the widely varying environmental temperatures. This is most acute in the case of the pursuit pilot who must don clothing on the ground for protection against very low temperatures to be encountered at high altitudes. Perspiration accumulates in the clothing at ground level temperatures, making the garment most uncomfortable and inefficient when cold temperatures are reached. The difficulty of providing ventilation for evaporation of moisture, sweat or insensible perspiration is obvious.

(b) The weight and bulkiness of clothing necessary to keep the body warm hampers the activity of the personnel. This especially concerns the hands which must be well protected and yet must perform numerous operations requiring tactile dexterity.

When nude, and in a resting condition, a man can maintain body heat without shivering at a minimum temperature of 82° to 84°F. When wearing a normal amount of clothing, under the same conditions, he can maintain heat balance at an environmental temperature of about 70° or 72°F. Thus normal clothing affords protection against a temperature drop of approximately 12°F.

The development of clothing for flying personnel which will afford insulative protection greater than four or five times that of normal clothing is impractical due to necessary limitations in bulk. The heaviest winter flying clothing developed, therefore, affords protection only four or five times greater than ordinary clothing and can be expected to maintain a man in heat balance, under resting conditions, down to a temperature of about +20°F. [82°F. − (5 × 12°F.) = 22°F.]. Below a temperature of +20°F., when wearing this clothing, heat balance can be maintained by increasing metabolism or heat production. By doubling or tripling heat production in the body, heat balance may be effected even at the very low temperatures encountered at high altitudes when wearing the heaviest equipment now available. Increasing heat production to maintain heat balance is not too desirable inasmuch as this necessitates a proportional increase in the amount of oxygen used and this life-sustaining gas is usually available in limited quantities on high altitude flights. Also, because of confined quarters or confining tasks, it is not possible for all airplane personnel to exercise to the extent which may be necessary to maintain heat balance. In such cases the body temperature declines until the shivering reflex is stimulated, producing an increase in metabolism which helps to maintain heat balance. The relatively large specific heat of the body is a mitigating factor in those cases where heat balance cannot be maintained. With a temperature decline of 1°C. the body gives up as much heat as is produced by it in 45 minutes at a resting rate of metabolism. Any unusual temperature fall in the body is, however, undesirable in view of the drowsiness which follows such experiences and which may become pronounced upon return to lower and warmer altitudes. This factor (large specific heat of the body) can be utilized only at the expense of the comfort and efficiency of flying personnel.

Thus, insulative clothing as a solution to the problem of maintaining body heat balance, in itself, has certain very definite limitations. The inadequate protection afforded against extremely low temperatures and the inability of some crew members to put on, or take off, clothing with the changing environment are among the more serious limitations to this solution.

### Third Solution

The third solution to the problem under consideration involves the use of heated clothing for maintenance of heat balance and protection against extremely low temperatures. Electrically heated clothing appears to be most adaptable for this purpose, and may be used in combination with varying amounts of insulative clothing.

#### *Advantages*

(a) The heat supplied can be adjusted to the requirements necessitated by outside temperatures, and

(b) The bulkiness of the clothing can be reduced to a minimum or to a degree which will permit normal activity and efficiency of the personnel.

#### *Disadvantages*

(a) Inadequate protection is afforded in case of failure of the power supply or in case of forced landing and abandonment of the ship on a cold terrain.

(b) A rather large amount of energy is needed for

each suit at extremely low temperatures even when insulative clothing of moderate weight is used in conjunction.

(c) A third disadvantage, and possibly the most interesting one from the physiologist's point of view, lies in the fact that the mechanisms normally responsible for heat balance in the body may be upset to such an extent by this mode of external application of heat that they cannot be depended upon to effect their normal warnings in connection with body temperature control. It is doubtful, therefore, if the individual's sense of comfort under such conditions can be relied upon to the extent that he can make proper adjustments with respect to the correct energy supply to his suit.

The reflexes which control vasoconstriction and motivate shivering to prevent too great a fall in body temperature originate, to an extent, in the surface areas of the body. Under conditions where the hands and feet alone, or in conjunction with other restricted body areas, are warmed artificially as in an electrically heated suit, these reflexes will be inhibited and a false sense of security established. Under such conditions it may well be possible for the internal body temperature to fall two or three degrees without causing any undue feeling of discomfort and without elicitation of the shivering reflex. Eventually shivering will likely occur and may be so severe when it does as to seriously impede the flier in the normal performance of his duty. These considerations are obviously more pertinent on long exposures than in the case of short exposures because of the longer drain on the body heat content.

The application of heat to all surfaces of the body together with proper distribution of the heat with respect to intensity will minimize the objections raised above. Sensations of comfort under such conditions cannot be expected to accurately mirror to a fine degree the state of the body with respect to heat balance but with proper distribution and application of heat, decreases in internal body temperature can be prevented.

## Summary

The final solution to the problem of maintaining body heat balance under the varied and extreme conditions encountered in flight is probably dependent to a great extent on future developments in airplane design. If pressure cabin airplanes are developed, the solution may lie in the heating of the cabin air together with some effective means of defrosting window areas in the cabin. As for the present, the best solution would seem to incorporate the best features of the electrically heated suit with the use of insulative clothing of maximum bulkiness commensurate with normal personal comfort and efficiency. Insulative clothing of moderate weight, such as the standard intermediate winter flying clothing, can be tolerated on all body areas except the hands which are needed for tactile operations. To keep the extremities warm and the body as a whole in heat balance, external heat could be applied with proper distribution beneath the insulative clothing. Heavy mittens could be carried as accessories or emergency equipment for protection in case of failure of the heating system or abandonment of the ship. This would provide adequate emergency protection, independent of the ship, for all except the most severely cold environmental conditions such as those encountered at very high altitudes and in the far north.

# The Design of Rotor Blades

R. H. PREWITT*

*Kellett Autogiro Corporation*

## Introduction

THE FACTORS THAT AFFECT the design of flexibly mounted rotor blades—that is, blades incorporating horizontal and vertical hinges—are practically the same for autorotating rotors and power-driven rotors insofar as knowledge of power-driven rotors has progressed to date.

The design of rotor blades may be divided into two parts: (a) determination of the physical dimensions and (b) detail design involving airfoil characteristics, including moment coefficient, chordwise center of gravity, blade weight, external smoothness, blade twist, thickness ratio, and internal structure. The two factors to be considered in determining the physical dimensions of the blades are blade loading and solidity (ratio of the blade area to disc area). The rotational tip speed varies as the square root of the blade loading; thus blade loading provides a convenient means for causing the maximum $L/D$ to occur at a given forward speed. With the same blade loading and all other factors equal, the maximum $L/D$ of a rotor increases with decreased solidity.

## General Aerodynamic and Design Considerations

### *Selection of Tip Speed Ratio for Maximum Efficiency*

Several autorotating rotors have been tested in full-scale wind tunnels. A 40-ft. diameter rotor was tested by the National Advisory Committee for Aeronautics at Langley Field, Virginia, in the full-scale wind tunnel several years ago. Fig. 1 shows the $L/D$ of this rotor plotted against tip speed ratio. It may be noted that the maximum lift-drag ratio occurs when the forward speed is 0.35 times the rotational tip speed, and the design should be such that it will take advantage of the tip speed ratio at which maximum lift-drag ratio occurs. For example, if it is desired to have maximum rotor efficiency occur at a cruising speed of 100 miles an hour, then 100 should be divided by 0.35 to produce the desired tip speed. This would give a rotational tip speed of 286 miles an hour or approximately 420 ft. per second. With further improvement in the design of the blades, the tip speed ratio at which the best $L/D$ occurs will probably be larger.

### *Rotational Tip Speed Variation with Forward Speed*

Flight tests of existing autogiros with blades fixed at optimum incidence show that the rotor speed increases as the forward speed increases. The following empiric equation gives this relationship for a range of tip speed from 0 to 0.4.

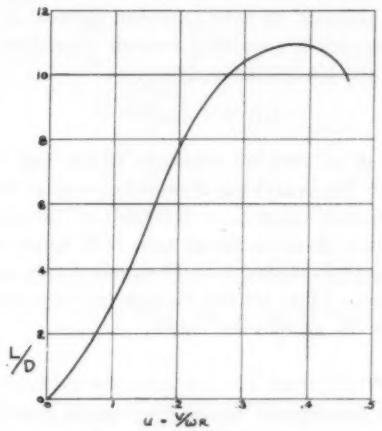


FIG. 1. Lift-drag ratio of rotor plotted against tip speed ratio ($\mu$).

$$\omega R = \omega_0 R(1 + 0.0021V) \qquad (1)$$

$V$ = forward speed in miles per hour
$R$ = blade radius in feet
$\omega_0$ = rotor speed in vertical descent (rad./sec.)
$\omega$ = rotor speed in forward flight (rad./sec.)

From the above relationship, the rotational tip speed at any given forward speed may be readily converted to the rotational tip speed in vertical descent. Thus in the preceding case, where a rotational tip speed of 420 ft. per second was obtained at 100 miles an hour, the rotational tip speed ($\omega_0 R$) in vertical descent will be 420/1.21 or 346 ft. per second.

### *Blade Loading*

The blade loading is a function of the tip speed, the air density, the slope of the lift curve, and the average weighted angle of attack of the blade sections, and the following equation is readily deducible:

$$BL = (\omega_0 R)^2 \rho a \alpha_L / 6 \qquad (2)$$

where $BL$ = blade loading in lbs./sq. ft.
$\omega_0$ = angular speed in rad./sec. in vertical descent
$R$ = radius in feet
$\rho$ = air density
$a$ = slope of the lift curve (degrees)

Presented at the Rotating Wing Aircraft session, Tenth Annual Meeting, I.Ae.S., New York, January 29, 1942.

* President in charge of Engineering.

$\alpha_L$ = average weighted angle of attack of the blade section

The angle of attack is dependent on the incidence or pitch setting of the blade, and numerous flight tests have shown that there is an optimum value of the angle of incidence of an autorotating blade. If the optimum value is used (as of course it should be)and if the air is assumed to have standard density, it is possible to employ a simplified empiric equation for determining the blade loading ($BL$).

$$BL = C_e(\omega_0 R)^2 \tag{3}$$

where $C_e$ is an empiric constant which can be used within wide lim ts and has a value between 0.00026 and 0.0003 (average value $C_e = 0.00028$). This coefficient is based on a theoretic blade area $bCR$ where $b$ equals the number of blades and $C$ equals blade chord at $3R/4$ radius. Thus, for the hypothetic rotor previously considered $BL = 33.5$ lbs./sq.ft.

***Blade Area***

Having determined the desired blade loading ($BL$) and knowing the gross weight ($W$) of the machine, the total blade area and blade dimensions may be readily determined from the following relationships:

$$\text{Blade area (total) } (BA)_T = W/BL \tag{4}$$

$$\text{Individual blade area } (BA)_T/b = CR \tag{5}$$

$b$ = number of blades.

If it is assumed that the gross weight ($W$) of the machine under consideration is 3,350 lbs., then the rotorplane will require a total blade surface area $(BA)_T$ of 3,350/33.5 equals 100 sq.ft.

***Blade Number and Dimensions***

Within reasonable limits, the number of blades comprising the rotor or the aspect ratio of the individual blades may be varied without affecting the final result. Aerodynamically, the most efficient rotor would be one that had the fewest number of blades and the longest blades for a given surface area. At the present stage of development, less than three blades in a rotor causes excessive vibration. Furthermore, when the machine is on the ground the blades droop excessively if the ratio of blade length ($R$) to blade chord ($C$) is greater than 20 to 25. In the hypothetic design carried out in this paper, it will be considered that there are three blades in the rotor and that the ratio of blade length to effective chord is 20. (In tapered blades having linearally varying chord from root to tip, the effective chord may be taken as the distance from leading edge to trailing edge at $^3/_4$ radius ($R$) for the usual case).

The following simple relationships then apply:

$$(BA)_T = bCR \quad R/C = 20 \text{ or } C = R/20 \tag{6}$$

$$(BA)_T = bR^2/20 \tag{7}$$

Substituting values in the hypothetic machine:

$100 = 3R^2/20$ or $R^2 = 2{,}000/3R = 25.8$ ft.
$C = 25.8/20 = 1.29$ ft., or $15^1/_2$ in.

***Rotational Speed of Rotor***

Having determined the rotational tip speed ($\omega_0 R$) in vertical descent and the blade radius ($R$), the rotation speed ($\omega$) of the rotor in vertical descent may be found by the following relationships:

$$\omega_0 = \frac{\text{rotor tip speed}}{R} \tag{8}$$

In the example given above, the rotor speed in vertical descent will be 13.5 radians per second or 129 r.p.m. The rotor speed at forward velocity may be found from the relationship given in Eq. (1).

***Inequality of Air Velocity, Flapping, and Angles of Attack***

On the advancing and retreating sides of a rotor in forward flight there is inequality of air velocity. This unequal distribution of air flow is illustrated in Fig. 2.

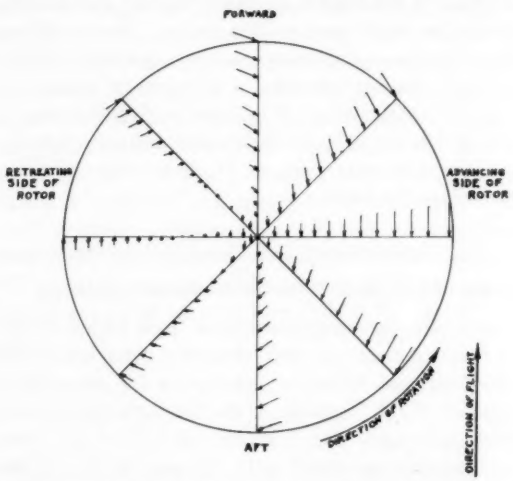


FIG. 2. Representative velocity and plan view direction of flow over rotor blades in eight phase positions at a tip speed ratio of 0.3.

There follows, with blades hinged about a horizontal axis, the well-known phenomenon of flapping, whereby lift moments on the advancing and retreating sides of the rotor are substantially equalized. On the advancing side of the rotor where the blades are flapping up, the blade elements are operating at a reduced angle of attack; on the retreating side of the rotor where the blades are flapping down, the blade elements are operating at greater angles of attack. As the forward speed of the machine increases, the blade elements on the advancing side of the rotor operate at increasingly smaller angles of attack and, conversely, the blade elements on the retreating side of the rotor operate at increasingly larger angles of attack. This is caused by increased flapping as a result of the greater disproportionate ve-

locities on opposite sides of the rotor with increased forward speed. Fig. 3[1] shows a plan view plot of the distribution of angles of attack of the blade elements of rotor.

### *Profile Drag*

The dispersion of the operating angles of attack of the blade elements tends to increase the average profile drag coefficient of the blade elements as the forward speed increases. It is, therefore, important to consider the angle of attack range for low values of profile drag coefficient of the blade airfoil, rather than to consider an airfoil from the standpoint of minimum profile drag coefficient at a given angle of attack. Because of the high air speed at the blade tips, consideration should be given to the use of ultra high-speed airfoil sections at and near the blade tip.

### *Selection of Thickness Ratio*

For the above reasons it is not desirable to use an airfoil section having too small a thickness ratio, and the thickness ratio should not be less than 10 to 12 per cent, depending upon the maximum tip speed ratio at which the blades will be operated. Since the inboard sections of the rotor have a relatively low rotational velocity, their profile drag coefficient is not so important as that of the tip sections and their thickness ratio may be greater. The inboard blade sections are subjected to the greatest stresses both when the blades are in the air and when they are at rest on the ground. Based on these considerations, it would appear that the thickness ratio of the inboard sections of the blade could be considerably greater than that of the outboard sections without much reduction in efficiency and with considerable improvements in structural characteristics.

### *Built-in Twist from Root to Tip*

The major difference between an autorotating rotor and a power-driven rotor so far as the design of blades is concerned is that in the former type there is a small flow up through the rotor and in the latter case there is a substantial downward flow through the rotor. Again, because of the relatively small flow up through the autorotating rotor, the blades may be built without twist and yet obtain optimum efficiency, while in the case of the power-driven rotor the blades will probably have a twist from root to tip similar to, but of less magnitude than, present engine propellers.

## Distribution of Air and Centrifugal Loads, Bending Moment Relief

### *Air Load Distribution*

When the blades are operating on the advancing side of the rotor, the combination of flapping or feathering and forward speed tends to bring the longitudinal center of pressure of the air forces inboard. Conversely,

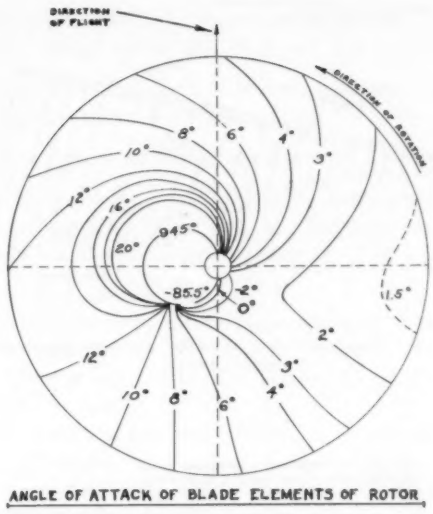


FIG. 3. Distribution of angles of attack for autorotating rotor in forward flight.

when the blades are operating on the retreating side of the rotor, the longitudinal center of pressure of the air forces acting on the blades tends to move outboard.

Figs. 4, 5, and 6 show the average distribution of the air forces acting on a rectangular rotor blade, the distribution of air forces acting on the advancing side of the rotor, and the distribution of air forces acting on the retreating side of the rotor, respectively. The center of pressure of the air forces is indicated by a heavy vector that shifts inboard on the advancing side and outside on the retreating side.

### *Distribution of Centrifugal Forces*

The normal components of the centrifugal forces acting on the blade elements at a given rotor speed are a function of the blade coning angle and the mass distribution along the span of the blade if the deflection or curvature of the blade is neglected. Fig. 7 shows the distribution of the centrifugal loads along the span for a blade having uniform mass distribution from root to tip. With uniform mass distribution, the centrifugal force on a mass element is proportional to the radius, and hence the centrifugal forces are triangularly distributed along the blade, and their center of percussion falls at two-thirds of the distance from the axis of rotation to the blade tip. Fig. 8 shows the two components of the resultant centrifugal force which are acting at the center of percussion of the blade. It will be noted that one component is perpendicular. The perpendicular or normal component opposes the air load which tends to lift the blade into a coned position.

### *Displacement of the Center of Percussion of the Centrifugal Bending Moment Relief*

If the blade, while coning, remained straight, there would be no change in the position of the center of percussion. If the center of pressure of the air load

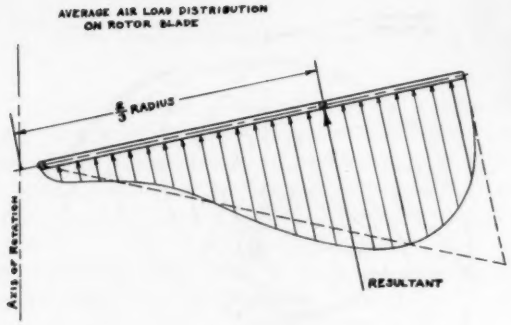


FIG. 4. Elevation view showing average longitudinal blade loading.

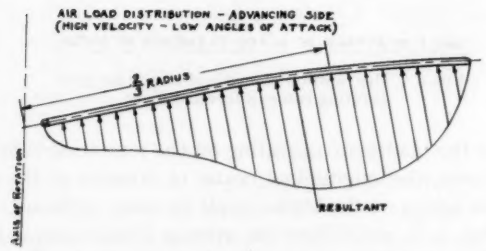


Fig. 5. Elevation view showing longitudinal blade loading on advancing side of rotor (note center of pressure moved inboard).

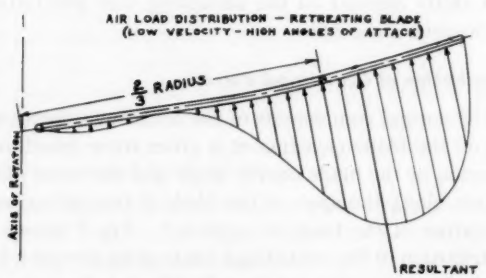


FIG. 6. Elevation view showing longitudinal blade loading on retreating side of rotor (note center of pressure moved outboard).

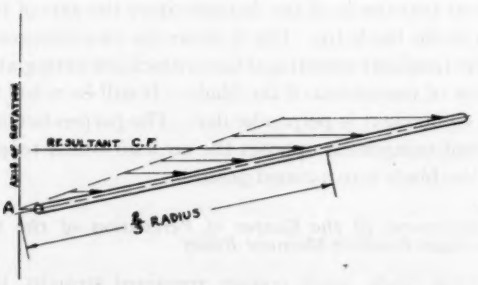


FIG. 7. Elevation view showing triangular distribution of centrifugal forces acting on coned blade having constant weight per unit length.

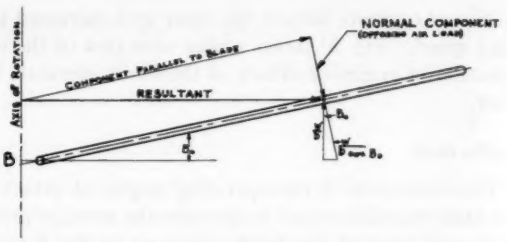


FIG. 8. Elevation view showing parallel and normal components of centrifugal force acting on coned rotor blade. The normal component of the centrifugal force opposes the air load $W/b \cos B_0$.

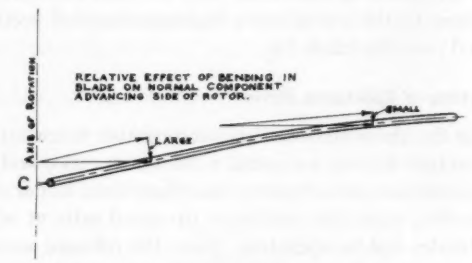


FIG. 9. Elevation view of rotor blade bowed down showing reduction in normal component of centrifugal forces toward blade tip. Bowing of blade caused by air forces on advancing side of rotor illustrated in Fig. 5.

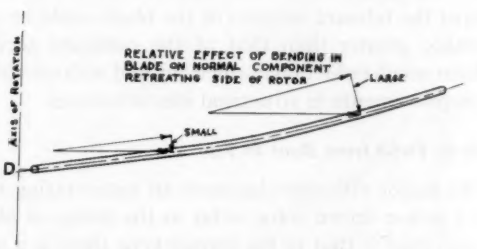


FIG. 10. Elevation view of rotor blade bowed up showing increase in normal component of centrifugal forces toward blade tip. Bowing of blade caused by air forces on retreating side of rotor illustrated in Fig. 6.

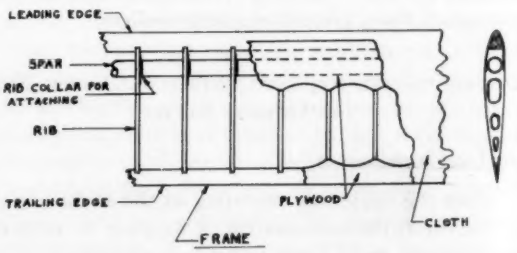


FIG. 11. Plan and section views of typical rotor blade.

always coincided with the center of percussion of the centrifugal forces, there would be little or no bending moments in the blade and no bending deflections in the plane of flapping. In actuality the shifting of the center of pressure of the air forces as illustrated in Figs. 5 and 6 introduces bending deflections in the blades in the flapping planes. Bending deflections in the flapping plane of the blades create a nonuniform variation in the distribution of the normal components of the elemental centrifugal forces acting on the blade.

Fig. 9 shows that the normal component of the centrifugal tension is reduced toward the blade tip when the blade is bowed down. When the blade takes this shape, the center of percussion of the normal components of the centrifugal tension moves inboard. It may be noted that an inboard shift of the air load which would produce the type of blade bending illustrated (Fig. 9) would tend to offset the inboard shifting of the normal components of the centrifugal force. In this manner the theoretic bending moments acting on a blade are considerably reduced in practice. For the above reasons a blade that is relatively flexible in the flapping plane will be subjected to smaller stresses than a more rigid blade.

Fig. 10 shows that the normal component of centrifugal tension is increased toward the blade tip when the blade is bowed up. In this case the center of percussion of the normal components of the centrifugal force moves outboard. When the blade takes the shape shown in Fig. 10, the air lift loads have moved outboard. Since the normal components of the centrifugal force increase toward the blade tip with increase in bow-up of the blade, the disproportionate increase in air lift toward the tip is automatically compensated by the increase in normal component of the centrifugal forces at the blade tip. An ideally designed blade might be one in which the maximum bending forces in flight would be equal—positive and negative.

***Weight of Individual Blades***

As an approximation, it may be assumed that the average center of pressure of the lift forces is coincident with the average center of percussion of the (opposing) normal component of the centrifugal forces. Based on this assumption, the weight of the blades required to produce a given average coning angle and rotor speed may be readily calculated in accordance with the following equations.

Referring again to Fig. 8, it may be noted that the normal component of the centrifugal force is equivalent to the opposing air load $W/(b \cos B_0)$ both assumed to be acting at a common center of percussion lying at $2R/3$ from the axis of rotation as illustrated in Fig. 7.

$$\text{Air lift moment} = 2RW/3b \cos B_0$$

(neglecting offset of horizontal hinge from axis of rotation)

$$\text{Centrifugal moment} = \text{centrifugal force} \times \sin B_0 \times 2R/3 = (MR\omega^2/2)(\sin B_0)(2R/3) = MR^2\omega^2 \sin B_0/3$$

Equating the air load and centrifugal moments, collecting the terms, and substituting $p/g$ for $M$:

$$p = 2gW/bR\omega^2 \sin B_0 \cos B_0$$

By assuming $\cos B_0 = 1$, $\sin B_0 = B_0$, and substituting the values given for $W$ in Eq. (4)[2], the total theoretic weight of the blades for a given rotor is:

$$bp = K_1K_2\sigma R^3/B_0$$

$W$ = gross weight of rotorplane (lbs.); $b$ = number of blades

$\omega$ = rotor speed in radians per second = $g$ = 32.2 ft./sec.[2]

$p$ = weight of one blade in lbs.; $B_0$ = average coning angle

$\sigma$ = ratio of blade area to disc area ($bC/\pi R$)

$K_1$ = a constant taken as unity but actually variable, depending upon the relative distribution of the air forces and centrifugal forces

$K_2$ = has the value $2\pi gC_e = 0.0566$

Taking the hypothetic design as an example, the weight of a blade would be $(2 \times 32.2 \times 3{,}350)/[3 \times 25.8 \times (13.5)^2 \cos B_0 \sin B_0]$. If it is assumed that the average coning angle is 7.50 in vertical descent, $\sin B_0$ is 0.13053 and $\cos B_0$ is 0.9914. The theoretic weight of an individual blade is 112 lbs.

The inboard structure of the blade, including reinforcement, extension links, dampers, etc., increases the theoretic weight of the blade by approximately 33.3 per cent, which in this case would give a weight for the individual blade of approximately 149 lbs., or a total weight for the three rotor blades of 447 lbs.

When means for varying the incidence angle of the blade during flight are included, the basic blade weight may be increased by 50 per cent in place of 33 per cent to account for the structure between the blade and hub, including the blade damper.

## Torsional Moments

The unsymmetric velocities and loads acting on opposite sides of the rotor may create cyclic changes in the torsional moment transmitted from the blade to the hub. These forces may arise from one or more of the following sources:

(a) If the moment coefficient of the blade airfoil section is other than zero, a torsional moment will be created which is proportional to the moment coefficient of the blade and the velocity of the airflow over the blade squared. This source of blade torsional moment may be eliminated by using a blade airfoil section having zero moment coefficient.

(b) The air forces acting on the blade may be considered as concentrated at the aerodynamic center, together with a moment coefficient about the aerodynamic center. The normal components of the centrifu-

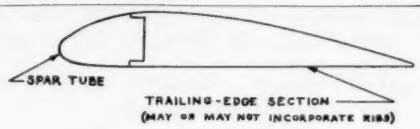


FIG. 12. Section view of promising metal-type blade construction. The nose is formed by irregularly shaped spar tube forming the outside contour at the leading edge of the blade. A light metal trailing edge is suitably attached to the formed leading edge.

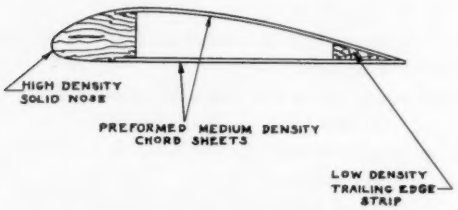


FIG. 13. Section view of promising wood- or plastic-type blade construction.

gal forces acting on the blade (opposing the air lifting forces) act downward at the chordwise center of gravity of the blade section. If this normal component of the centrifugal forces is not directly opposed by the air lift forces, a torsional moment will be created which is equivalent to the product of the lifting force produced by the blade and the distance between the chordwise center of gravity and the aerodynamic center of the blade. This torsional moment may be eliminated by designing the blades so that the chordwise centers of gravity are coincident with the aerodynamic centers of the blade sections.

(c) There is another minor source from which torsional moments may be transmitted from a blade to its hub. As explained above, rotor blades flex in the plane of flapping cyclically with rotor speed. This flexing of the blade creates a shear force at the root of the blade which may be represented by a reaction normal to the longitudinal blade axis in the plane of flapping. If the control axis for the blade or hub does not lie on the projection of a line through the aerodynamic centers and chordwise centers of gravity, then a cyclic moment will be transmitted between the blade and hub. This force may create a cyclic change in the blade angle.

(d) When a blade is bowed as illustrated in Figs. 9 and 10, the blade diverges away from the fixed center line of the blade root section. In a power-driven rotor the drag forces acting on the bowed blade in combination with the imput torque forces which are transferred to the blade in a plane through the center line of blade root creates a torque force on the inboard end of the blade. To a lesser degree these torque forces are created in autorotating rotors. In an autorotating rotor incorporating straight blades, the inboard blade elements exert a driving force, whereas the outboard blade sections are at smaller angle of attack than the inboard sections and therefore create a drag force on the blade.

## SEVERAL TYPES OF CONSTRUCTION

(a) The most general type of blade construction consists of plywood and/or cloth covered contour ribs mounted on a steel tubular spar every 3 or 4 in. along the blade span. The cover carries the air loads to the ribs which in turn transfer the air loads to the spar tube which is the main structural member of the assembly. Lightning holes are usually cut in the web of the $^1/_4$ in. plywood ribs aft of the spar to maintain a forward location of the chordwise center of gravity of the blade. Fig. 11 shows a blade section of this type construction.

(b) Another type of construction which has been tried experimentally consists of an odd-shaped spar tube drawn to form the nose of the blade section to which is attached a trailing edge section. This type construction is sectionally illustrated in Fig. 12.

(c) Plastic impregnated wood has also been used experimentally for construction of rotor blades. In this case a highly compressed heavy density (1.4) wood impregnated leading edge member is machined to contour. To the leading edge member are attached preformed chord plywood sheets of lesser density (0.8). A triangular trailing edge strip of light wood is sandwiched between the preformed plywood chord members. There are no ribs in this construction, although the addition of ribs might improve the structure. A section showing the plastic impregnated type blade is illustrated in Fig. 13.

## REFERENCES

[1] Bailey, F. J., Jr., *Photographic Observations in Flight of the Stalling of Rotating Wings*, Rotating Wing Aircraft Meeting, Philadelphia, Pa., 1939.

[2] Prewitt, R. H., *Possibility of the Jump-Off Autogiro*, Journal of the Aeronautical Sciences, Vol. 6, No. 1, pp. 10–14, November, 1938.

# The Ability to See Low Contrasts at Night

MATTHEW LUCKIESH* AND FRANK K. MOSS†
*General Electric Company*

IN DEVELOPING and standardizing a test for determining the ability of military personnel and others to see under low brightness levels such as those often present in night flying, it is a logical assumption that the ocular examination should be conducted with brightnesses that are photometrically comparable to those encountered in actual observation. Under so-called blackout conditions, for example, most visible objects are large in visual or angular size and low in brightness contrast with respect to their backgrounds. Therefore, a low-contrast test chart illuminated to some scotopic brightness is indicated for test purposes. Under such a low brightness, colors are not recognized and only the rod system of the retina is effective in seeing. These are prerequisites if the ocular tests are truly to reveal the ability of the examinee to see objects of low contrast at night. Obviously, the usual clinical measures of visual acuity, involving photopic brightnesses and maximal-contrast test objects, do not meet these axiomatic requirements of an appropriate night-vision screening test.[1] In general, photopic brightness levels are high enough to permit the recognition of colors, and seeing is considered to depend upon the retinal cones instead of the rods alone.

The inadequacy of the usual criterion of visual acuity in revealing differences among individuals in ability to see at night is clearly shown by the data of Table 1 for two brightness levels. These data summarize 150 monocular examinations made with the 1932 A.M.A. Test-Chart illuminated to brightness of 10 and 0.01 foot-lambert,‡ respectively. Obviously, these measurements could have been made under an even lower scotopic brightness level although *not* with equal facility. It will be noted that 117 of the 150 cases were rated alike and superior in visual efficiency or visual acuity by tests made under a brightness level of 10 foot-lamberts, while only 11 of the 150 cases were rated alike and superior in visual efficiency under a brightness level of 0.01 foot-lambert. These data also indicate that the spread in visual efficiency among these subjects is nearly doubled when the chart brightness is reduced from 10 to 0.01 foot-lambert. In interpreting the data pertaining to the A.M.A. rating of visual efficiency, it should be recognized that the range between 100 and zero represents the difference between normal vision and blindness.

The use of test objects of maximal contrast (black on white) in so-called screening tests for selecting military and other personnel involves the tacit assumption that individual differences in contrast sensitivity are unimportant, while differences in the resolving power or the visual acuity of the eye, as determined with objects of maximal contrast, are of primary importance. However, this is not entirely true and the hazards of these assumptions do not have to be risked, since the ocular examinations can readily be made with low-contrast test objects, such as light gray objects on a white background. There are many sound reasons for using a chart comprising a progressive series of low-contrast test objects. Such a chart is capable of revealing individual variations not only in absolute sensitivity to brightness but also to variations in contrast sensitivity or sensitivity to brightness difference.[3] The latter visual characteristic is primarily important in observation at night and, obviously, it is not reliably measured with test objects of maximal contrast, such as black test objects seen against a white background or completely silhouetted against a luminous background.

The Luckiesh-Moss Low-Contrast Test-Chart,[1] illustrated in Fig. 1, consists of pairs of digits of modified Snellen design photographically reproduced in various degrees of contrast with their white backgrounds. Obviously, this chart represents merely one of many possible forms and ranges of contrast based upon the same basic principles. It is emphasized that Fig. 1 was made from a photographic reduction and that the exact and fine gradation in brightness contrast of the actual chart suffers so greatly that Fig. 1 is *merely* an illustration. The original chart is about 20 in. long. In the present form of the low-contrast chart, the test objects are approximately equivalent in size to 20/140 Snellen (2.44 in. overall) characters when the chart is viewed from a distance of 10 ft. However, the size

TABLE 1

The Values Pertaining to "Visual Efficiency" Are Those Adopted by the American Medical Association[2] and Are Directly But Complexly Related to Corresponding Measures of Visual Acuity

| 10 Foot-Lamberts (Photopic Vision) | | | 0.01 Foot-Lambert (Scotopic Vision) | | |
|---|---|---|---|---|---|
| Visual Efficiency | Snellen Rating | Number of Cases | Visual Efficiency | Snellen Rating | Number of Cases |
| 100 | 20/20 | 117 | 85 | 20/38.4 | 11 |
| 95 | 25.7 | 15 | 80 | 44.9 | 5 |
| 90 | 32.1 | 14 | 75 | 52.1 | 43 |
| 85 | 38.4 | 3 | 70 | 60.2 | 40 |
| 80 | 44.9 | 1 | 65 | 68.2 | 19 |
| | | | 60 | 77.5 | 20 |
| | | | 55 | 86.8 | 4 |
| | | | 50 | 97.5 | 8 |

* Director, Lighting Research Laboratory.

† Physicist, Lighting Research Laboratory.

‡ A foot-lambert is the brightness of a perfectly diffuse and perfectly reflecting surface (100 per cent reflection factor) when illuminated to 1 foot-candle.

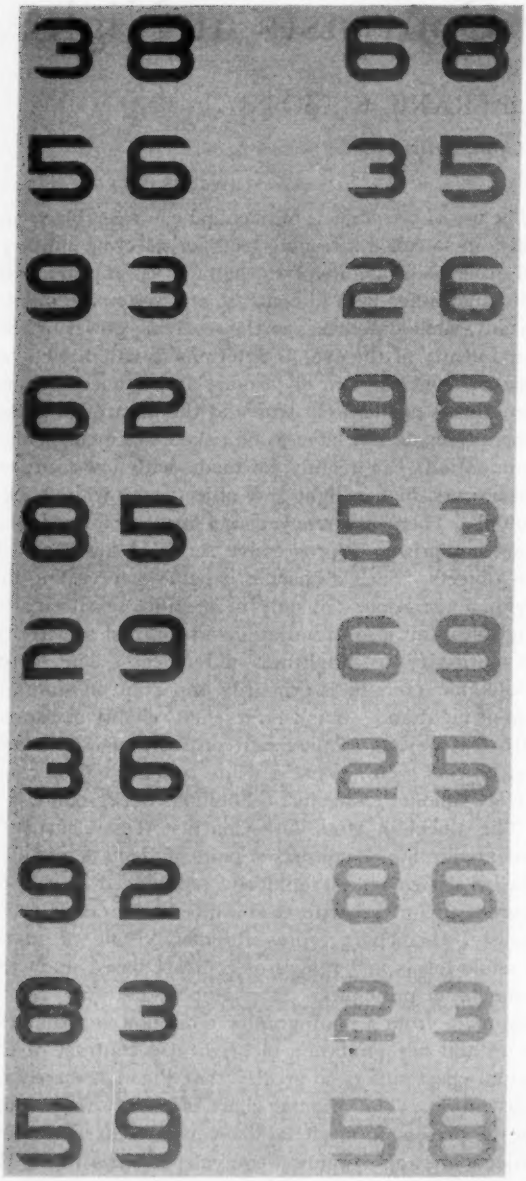


FIG. 1. This is merely an illustration, not a reproduction for actual use, of the Luckiesh-Moss Low-Contrast Test-Chart. The original, produced carefully by photography, is calibrated in terms of the degree of contrast between test characters and their white background and is about 20 in. long.

of each digit was carefully determined so that all of the digits used are equal in visibility for the same degree of contrast. Since the two-digit combination must be read correctly, the probability of guessing the correct number is obviously quite low. The series of objects of the present chart varies from a maximum of about 40 per cent in contrast to a minimum of about 10 per cent in contrast. This has been found satisfactory at ordinary brightness levels and also for a brightness level as low as 0.01 foot-lambert.

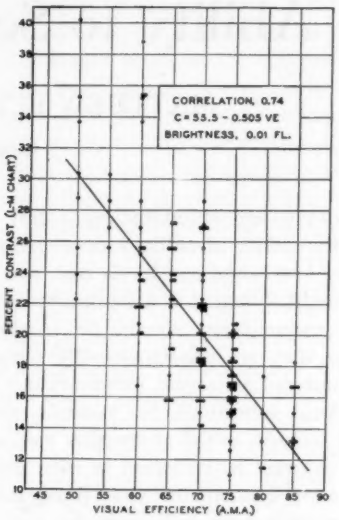


FIG. 2. The correlation between measurements of visual function determined from contrast thresholds (ordinates) and visual acuity thresholds (abscissas), respectively.

The data presented in Fig. 2 summarize 150 monocular examinations made with the 1932 American Medical Association Test-Chart and the L.-M. Low-Contrast Test-Chart, with both charts illuminated uniformly to a brightness of 0.01 foot-lambert. The eyes of each subject were adapted to this brightness for a period of 30 min. in each case. It will be noted from Fig. 2 that the correlation between the two sets of data thus obtained is 0.74. This fact per se is an indication of the difference between the two tests of night vision. If they were in perfect agreement, it follows that a correlation of 1.00 would have been obtained. It will be noted (1) that the subjects possessing the *same* visual efficiency (A.M.A. Chart) varied markedly in their ability to recognize low-contrast objects (L.-M. Chart) and (2) that the variation in contrast sensitivity among the group possessing the highest rating in visual efficiency or acuity is about as great as it is for the group with the lowest rating. It will also be noted, for any given group, that those possessing the greatest ability to see under a brightness of 0.01 foot-lambert were able to recognize objects having a brightness contrast only about one-half as great as those recognizable by the subjects of the same group who possessed the least ability to see. Thus, many objects that would be visible to some subjects of a given group, as determined by the criterion of visual efficiency or acuity, would not be seen by others of the same group.

On the basis of visual efficiency, it will be noted from Fig. 2 that 11 cases showed a visual-efficiency rating of 85 per cent under the low level of brightness that prevailed during these tests. Thus, it might be concluded that these subjects would excel, as night observers, all subjects who possessed a lower visual-efficiency rating. However, it will be noted that many of the subjects

possessing a lower visual-efficiency rating would excel, some having a higher rating in their ability to recognize low contrasts under low brightness levels. Correspondingly, certain subjects who might be eliminated as night observers by the criterion of visual acuity might easily qualify when examined directly with respect to their ability to see low contrasts under low brightness levels. A critical examination of Fig. 2 from this point of view is particularly interesting.

The selection of a brightness of 0.01 foot-lambert as the low brightness or scotopic level for these tests was based upon both theoretic and empiric considerations. At this brightness level, seeing depends almost entirely upon rod vision. Hence, this level is theoretically appropriate for a screening test designed to detect individual differences in ability to see under low levels of illumination. A brightness level of 0.01 foot-lambert is also comparable in order of magnitude with the brightnesses of roads and highways under moonlight. Thus the data obtained under 0.01 foot-lambert are readily interpretable in many practical situations without introducing the uncertainty of extreme extrapolation.

Although a brightness level lower than 0.01 foot-lambert might be used, it would increase the time required for reaching a reasonably stable state of retinal adaptation. Thus, for the practical purpose of testing many subjects, it is desirable to use the highest scotopic brightness that will yield adequate data. On the other hand, as the brightness level is decreased, the contrast sensitivity of the subject diminishes and higher contrast test objects are required for discernment. Thus, the test becomes less appropriate as a means of appraising contrast sensitivity. Actually, the test objects of the present L.-M. Chart cannot be seen by subjects possessing normal vision when the background has a brightness as low as 0.001 foot-lambert. Obviously, if the reduction in brightness level were carried to an extreme, these tests would also yield data on the thresholds of brightness discrimination. However, it is not probable that such data would add materially to the value of screening tests for the purposes indicated. It should also be recognized that no single low brightness level is ideal or entirely free from criticism from both theoretic and practical points of view. With this in mind a brightness level that minimizes the time required for the test and still yields adequate information is the most practicable.

## References

[1] Luckiesh, Matthew, and Moss, Frank K., *Contrast Sensitivity as a Criterion of Visual Efficiency at Low Brightness Levels*, American Journal of Ophthalmology, Vol. 22, p. 274, 1939.

[2] Report of the Committee on Compensation for Eye Injuries, Section on Ophthalmology, American Medical Association, 1925, pp. 368–377.

[3] Luckiesh, Matthew, and Moss, Frank K., *The Science of Seeing*, D. Van Nostrand Company, New York, 1937.

Aeronautical circus posters.

Aeronautical dime novels.

# Aeronautical Archives Exhibit at University Club in New York

At the request of the University Club of New York, a selected exhibit of artistic and historical aviation material from the files of the Aeronautical Archives of the Institute was shown in the main lobby of the Club throughout the month of March. It was regarded as one of the most attractive and timely exhibits ever shown at the Club and drew many expressions of interest and appreciation from its members and their guests.

Since the spacious foyer of the Club provided an exceptional opportunity to display some of the more interesting items in the extensive collections now in the Archives, photographs of a few

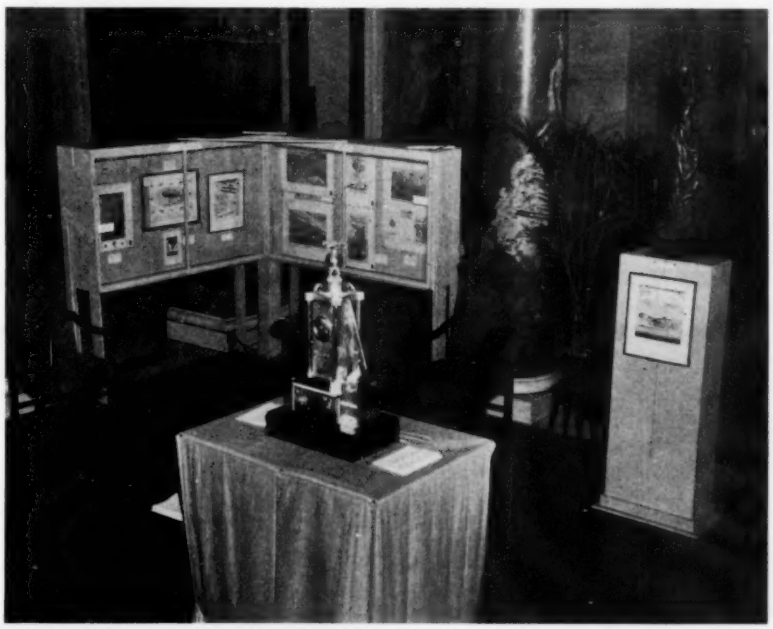

Two of the sixteen exhibit cases of the Aeronautical Archives at the University Club (N.Y.). Center—The Edwin Musick Trophy. Right—The Gordon Bennett Balloon Trophy.

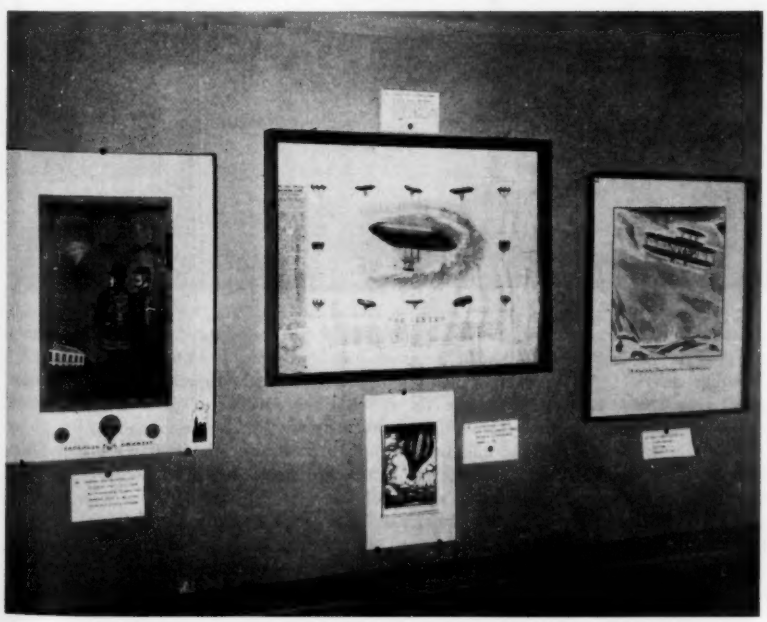

Left—Japanese mission witnessing flight of T. S. C. Lowe's balloon at Philadelphia (1861). Center—Dr. Solomon Andrews' airship that flew over New York City in 1863. Below—Blanchard's flight in 1793. Right—The Orville Wright flight at Kitty Hawk, December 17, 1903.

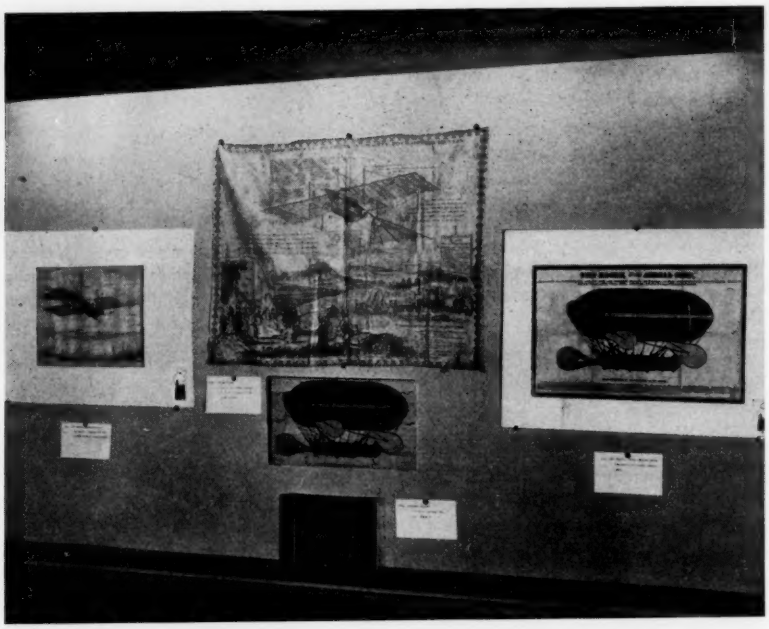

Fabric, prints, and early jigsaw puzzle of Henson's *Aerial Steam Carriage* (1843) and Count Lennox's *Aerial Ship Eagle* (1835).

Aeronautical music from the Bella C. Landauer collection in the Archives.

of the exhibits are reproduced here in order that Institute members may obtain some idea of the nature and extent of the valuable gifts received in recent months.

The art work included prints and engravings by such famous artists as Goya, Mergun, Doré, Pennell, and Daumier, etchings by modern artists, bookplates designed for private aeronautical libraries, and medals and commemorative medallions. The old prints, posters, book illustrations, and sheet music covers show the influence that the balloon age and the predicted advent of heavier-than-air flying machines exerted on the art and literature of the past.

Some of them depict historical events in aviation, such as the rare print of the flight of "The Aereon of Dr. Solomon Andrews" over New York City, which was loaned for this exhibit by Arnold W. Knauth, the great-grandson of the inventor. Others describe amusing, fanciful and, for the times, satirical ideas on the methods of future air travel. The covers and illustrations for the dime novels demonstrate by far the greatest latitude for uninhibited imagination, but it is not improbable that these thrillers stimulated many of the boys of the 1880–1890 period to become the practical airmen of the next century.

Most of the material exhibited was donated by Mrs. Bella C. Landauer and Mr. Harry F. Guggenheim. Within the past month Mrs. Landauer has given to the Archives the remainder of her entire collection—the greatest of its kind in the world.

# Institute Notes

## Martin Addresses Detroit Section

The Engineering Society of Detroit and the local Section of the Institute held their second joint meeting of the year at the Rackham Educational Memorial Building in Detroit on Wednesday, April 8. Glenn L. Martin, President of The Glenn L. Martin Company and Past-President of the Institute, spoke on "Aircraft in Peace and War."

The dinner in his honor at the Rackham Building before the lecture was attended by over 400 persons. Despite the fact that this meeting was limited to members of the Institute and the Engineering Society, an audience of a thousand in the main auditorium heard the lecture, excerpts from which are given below:

### Aircraft in Peace and in War

The airplane has forced itself into world consciousness with meteoric swiftness. I need not detail the circumstances that have brought this phenomenon; they are all too well known. But the tremendous air movements—the destruction of cities, of armed forces, forts, battleships—make logical the questions so often asked: "What's next? What is ahead for aircraft in peace and in war?"

Let me begin by saying that I am not a military expert; I have never pretended to be. But a lifetime spent in the design and production of military aircraft has brought some conclusions pertinent to our considerations here. Back in 1913 it was my privilege to help conduct the Army's first bombardment experiments at San Diego. So fascinated was I with the airplane's demolition possibilities that I made this statement, culled from the newspapers of August 7, 1914, which were headlining the beginning of World War I:

> "The aeroplane will practically decide the war in Europe. Veritable flying death will smash armies, wreck mammoth battleships, and bring the whole world to a vivid realization of the awful possibilities of a few men and a few swift aerial demons. For the old-time war tactics are no more. The generals who realize this quickest and fight first with the flying death, will win."

I was one war too early on that one. But today we find air forces the most powerful influence in victories; lack of them, the outstanding cause of defeats. On the evidence, I must assert that no armed force can be successful on any major project without air supremacy in its theater of war.

I venture to say that too few people understand the power of the airplane—or, rather, the fleet of airplanes—as long-range artillery. Let us illustrate with a hypothetic mission.

Word arrives at a battleship station that a hostile force has been sighted 1,000 miles away. The battleship is stocked with supplies and ready for battle. In 38 hours, if the target has not moved too far, the first salvo of nine tons of explosives will be fired at the target. Now a fleet of 150 bombers, costing about the same as a battleship, gets word of the force 1,000 miles away. In six and a half hours, these airplanes discharge 750 tons of explosives on the target. In 38 hours, 2,250 tons of bombs will have fallen on the objective. Even a continuous cannonade from the battleship could not approach the destructive power unleashed by the air fleet.

Again, the extreme mobility of great naval air forces would answer in large part the desperate need we now find for a two-ocean navy. The plight of a one-ocean navy decoyed into the wrong ocean at the wrong time can well be imagined. A powerful air force, however, can serve in either ocean in full strength on short notice, without worrying about the Panama Canal.

This war has sold ocean air transport to the world. Today, people (at least, those who can get passage) step aboard the Clipper ships without a qualm and with a perfect feeling of security. They step aboard surface ships in fear and trembling of the skulking submarines. Yet the record shows that organized airline travel not only has been the safest means of transport since the war began but that it was safer for several years before the war. In the future it will be safer yet, largely because of developments unfolding during this war period.

We are heading for winged vessels larger than any of which we have yet dreamed. Transoceanic air operations, now being conducted so successfully by our American companies, are presently based on aircraft having a maximum gross weight of between 82,000 and 84,000 lbs. These flying boats can carry a pay load of about 4,000 lbs. a distance of between 3,000 and 4,000 miles, depending on headwinds and the amount of fuel reserve needed. Such performance is an outstanding technical achievement which was considered impossible a very few years ago. Passenger accommodations in these airplanes are excellent.

But these aircraft are inconsiderable, indeed, compared with the flying ships we are already planning. I can tell you that my Company already has plans for a 250,000-lb. commercial air vessel. And I can tell you also that our studies have, as a matter of fact, shown that no technical considerations limit the size of airplanes that can be built; the only limit is the amount of payload available per trip. Indeed, we should be able to build 500,000-lb. airplanes in a very few years.

The size of aircraft and possible limitations in their weight have been discussed many times. For every considerable increase in the size of airplanes there have always been experts who say "it can't be done." Such disbelief is based invariably upon assumption of current engineering data. We would not project our 250,000-lb. boat unless we knew that engines and propellers and advances in aerodynamic and hydrodynamic design were available to make such a ship technically feasible. Nor would we project it if we had any doubt that it is both economically possible and economically feasible.

The determining factor is the availability of payload. Of that traffic in the postwar period I am confident. I am certain that air freight, domestic and foreign, will become a very important part of our commerce when the war is over. It has been hampered in the past by restrictions and monopolies, and its first tottering steps were halted by hostilities. Such transport is not only economically feasible but it offers a speed of which modern business will not long deprive itself. When one considers what outmoded old airplanes have been doing for several years in South America—delivering mining machinery, tractors, and supplies and taking out rich resources from roadless and railless regions—he begins to appreciate what vast possibilities lie in the North American and transoceanic fields. Indeed, he appreciates what a part the modern air freighter will play in opening up rich new resources to replace our strained supplies of raw materials.

The Army has done more to develop air freight than any other operator, and it is suprising to some people to discover that in the last several years the Army has carried more cargo by air than all the airlines of the United States put together.

That all first-class mail will travel by air in the future peace is a foregone conclusion. It has been a long time coming, but it is historically true that the mails have always found their way into the fastest means of transport available, although never without a fight. The stage-coach operators fought the pony express. The barge men fought the railroads. But always the mails have gone through—fast.

That domestic air travel will boom after the war is another reasonable conclusion. The great safety record hung up by the airlines in the last several years continues. Air travel in the war is

filling every available seat, and people are irked at being turned away from the ticket windows. It is human nature to want what you are denied. Besides, hundreds of thousands of men, trained to the air by the war, will be able to see no other means of transport when they return to peaceful pursuits.

But the spectacular development, I repeat, will be in the ocean field—in the field of flying ships that will grow larger and larger. With them we shall rehabilitate a weary world, draw it closer together, re-establish the broken threads of commerce, cross the last frontiers of isolation.

## Los Angeles Section Elects Officers

At a meeting held at the Hollywood Roosevelt Hotel, March 10, new officers for the Los Angeles Section were elected as follows: Chairman—W. C. Rockefeller, Chief of Aerodynamics, Vultee Aircraft Inc.; Vice-Chairman—Clarence L. Johnson, Chief Research Engineer, Lockheed Aircraft Corp.; Treasurer—Carl W. Babberger, Chief of Aerodynamics, Hughes Aircraft Co.; and Secretary—Walter C. Clayton, Chief Engineer, Curtiss-Wright Technical Institute.

The retiring officers are: Dr. A. L. Klein, Chairman; W. C. Rockefeller, Vice-Chairman; Eugene Root, Treasurer; and R. L. Thoren, Secretary.

At this meeting Dr. Klein presented a paper on "Some Principles of Production Design."

## News of Institute Members

**W. E. Baptist,** M.I.Ae.S., who has been Chief Inspector, Airscrew Division of the De Havilland Aircraft Co. Pty. Ltd., of Australia, is now Chief Inspector in the Aircraft Parts Division, National Motor Springs Pty. Ltd.

**Paul M. Butman** has been commissioned a 2nd Lieutenant in the Army Air Forces.

**Lt. E. W. Conlon, U.S.N.R.,** A.F.I.Ae.S., is on active duty with the Navy Bureau of Aeronautics in Washington. He is on leave of absence from the University of Michigan where he was Associate Professor of Aeronautical Engineering.

**Alfred R. Crisi,** who was until recently in training as an Aviation Cadet in Meteorology, is now 2nd Lieutenant in the Army Air Forces, serving as a Base Weather Officer at a post in Georgia.

**George W. DeBell,** A.F.I.Ae.S., recently on the engineering staff of The Glenn L. Martin Co. where he had specialized in studies on the use of plastic materials in aircraft construction, is Chief Engineer of The Thomas Mason Co., Stamford, Conn. He had been an Engineer with Fleetwings, Inc., and prior to that had been Chief Engineer of Fairchild Aircraft Corp.

**Harry S. Egerton** has left Lockheed Aircraft Corp., where he was Power Plant Layout Engineer, to join Kellett Autogiro Corp. as Senior Design Layout Engineer.

**Joseph V. Foa,** M.I.Ae.S., formerly Instructor in Aeronautical Engineering at the University of Minnesota, has been appointed Chief Engineer of American Aero-Marine Industries, Inc., New Bedford, Mass.

**Walter F. Hagman** is now Assistant Works Engineer, Bethlehem Steel Co., in Chicago. He was previously Senior Design Engineer with Lockheed Aircraft Corp.

**Everett Hannifin** is now employed at Boeing Aircraft Co. as Junior Flight Test Equipment Engineer.

**Walter B. Howard, Jr.,** who had been an Associate Engineer at the Jacksonville Naval Air Station since last July, is now a 1st Lieutenant in the Army Air Forces assigned to the Central Procurement District in Detroit.

**Milton D. Hunnex,** formerly Weight Control Engineer, Lockheed Aircraft Corp., has joined the staff of Cal-Aero Corp. as an Instructor.

**Edward J. Ill** has left the AGA Aviation Corp., where he was Weight and Balance Engineer, to become Aviation Sales Engineer in charge of aircraft subcontracting for the Orange Screen Co., Maplewood, N. J.

**Burnham Litchfield,** M.I.Ae.S., has resigned as Vice-President and General Manager of Allied Aviation Corp., and is now Sales Manager for Duramold Aircraft Corp., a subsidiary of Fairchild Engine & Airplane Corp.

**Samuel J. Loring,** M.I.Ae.S., Research Engineer with Vought-Sikorsky Aircraft Div., United Aircraft Corp., received the Wright Brothers Medal for 1941 awarded by the Society of Automotive Engineers for the best paper on an aeronautical subject read at any of its meetings during the year. Presentation of the medal was made at a meeting of the S.A.E. in New York on March 13 by **Dr. J. C. Hunsaker,** Hon.F.I.Ae.S., Chairman of the N.A.C.A., who is chairman of the Wright Brothers Medal Board of Award.

**Dr. W. Randolph Lovelace,** A.F.I.Ae.S., Surgeon at the Mayo Clinic and Flight Surgeon and Major in the Army Medical Corps Reserve, is on active duty at the Office of the Air Surgeon in Washington where he is serving as Director of Physiologic Research and Consultant in Surgery to the Army Air Forces. He recently became a member of the American Board of Surgery.

On April 1 **John M. Luther,** M.I.Ae.S., joined the staff of Globe Aircraft Corp., Fort Worth, Tex., as Assistant Chief Engineer. He had previously been a Wing Group Leader with the Airplane Div. (Buffalo Plant), Curtiss-Wright Corp.

**Raymond B. Maloy,** M.I.Ae.S., has been promoted from Associate to Aeronautical Engineer with the C.A.A. He is on the staff of the Aircraft Engineering Division.

**J. H. Millar,** M.I.Ae.S., formerly Managing Director, Aviation Corporates Ltd., and Director, Engineering Developments (England) Ltd., is a Lieutenant in the Royal Navy Volunteer Reserves and is now assigned to the Royal Navy Office of the British Air Commission in Washington.

**Joseph D. McCarthy** has been an Engineer with The Glenn L. Martin-Nebraska Co. since the first of the year. He was previously an Inspector for Consolidated Aircraft Corp.

**Allen H. McCormick** has left the Experimental Assembly Dept. of Pratt & Whitney Aircraft Div., United Aircraft Corp., to take a position in government service.

**T. Edward Moodie,** A.F.I.Ae.S., General Manager of the Traco Div., M. A. Ferst, Ltd., is Vice-President and Chief Engineer of Aviation Engineering, Inc., a company recently organized in Atlanta for the manufacture of plywood aircraft components.

**Dr. Norton B. Moore,** A.F.I.Ae.S., formerly Chief Research Engineer for the St. Louis Plant of the Curtiss-Wright Corp. Airplane Division, has been appointed Director of Aerodynamic Research for the Research Branch of the entire Airplane Division with headquarters at Buffalo.

**Charles W. Neff,** recently an Inspector for Consolidated Aircraft Corp., is now a Design Engineer with Emerson Electric Mfg. Co.

**Herbert L. Stevens,** M.I.Ae.S., who had been Deputy Director of Air Technical Services for the British Air Commission in Washington for the past year, has returned to England to take the post of Deputy Director of the Royal Aircraft Establishment.

**Godfrey B. Speir,** M.I.Ae.S., has left the Patent Dept. of Wright Aeronautical Corp. to go on duty as a Captain in the Army Ordnance Dept. He is stationed at the Aberdeen Proving Ground.

**David B. Thurston** has joined the Experimental Design Dept. of Vought-Sikorsky Aircraft Div., United Aircraft Corp., as a Design Engineer. He was previously an Assistant to the Project Engineer, Brewster Aeronautical Corp.

## Student Branches

**Boeing School of Aeronautics.** The following officers for the current school term were elected at a meeting on February 10: Chairman—John Jones; Vice-Chairman—Charles Glyssin; and Secretary-Treasurer—Curtis Dunwoody.

**Casey Jones School of Aeronautics.** Branch officers for the spring term, elected at a meeting on February 28, are as follows: Chairman—Donald B. Fishbeck; Vice-Chairman—James J. Maloney; Secretary—Walter J. Engert; Treasurer—Donald E. Marcmann; Sergeant at Arms—Jung Git Chung; and Corresponding Secretary—George I. Hackenberger. The new officers were inducted at the first meeting of the new term on March 20, at which time plans were made for the activity of the Branch for the next six months.

**Duke University.** Twenty-five members of the Branch attended a meeting held on April 9 and presided over by Chairman James Lee Fisher, Jr. N.A.C.A. motion pictures on a smoke-flow wind tunnel and the free-spinning tunnel were shown. A program innovation was introduced with an aeronautical question-and-answer contest in true radio quiz style, complete with 64-cent "jackpot" questions. The quiz concluded with an open contest to determine the identity of airplanes pictured on a screen.

**Indiana Technical College.** At a meeting held on March 30 a brief résumé of each of the papers presented at the recent Midwest Student Branch Regional Meeting was given by Jack Murray. Ray Trout reported on the program at the Regional Meeting banquet. Reports were received from various chairmen of Branch Committees. Tom Millard stated that a special speaker on Industrial Management would be obtained for a future meeting of the Branch. Malcolm Goodenough indicated that progress had been made toward carrying out a plan for contacting all graduates of the Aeronautical Department of Indiana Technical Institute. Norman Cosner outlined the program for future meetings and the papers to be presented by Student Members. The Motion Picture Committee announced that a sound projector had been purchased for the use of the Branch and of other student organizations at the College.

Two papers were read at this meeting: Malcolm Goodenough discussed the design of high-speed military planes and James Glascock gave a report on factors limiting the ultimate speeds of airplanes. After a recess, the meeting was concluded with the showing of several motion-picture films.

**Polytechnic Institute of Brooklyn.** This Branch has held eight meetings throughout the school year, 1941–1942, under the direction of the following officers: Paul Libby, Chairman; Ross Fleisig, Vice-Chairman; Frank Marciniak, Secretary-Treasurer; and M. Mandel, Corresponding Secretary.

At the meeting on March 5, William Preston, '42, spoke on "Experiences at Pratt and Whitney." Eugene S. Davidson, '42, was the speaker at the next meeting on March 19. His topic was "The Wright Brothers and Langley." The Branch plans to hold its Annual Banquet on April 22.

**Rensselaer Polytechnic Institute.** On March 26 two motion pictures were shown before the members of the Branch: "Internal Combustion Engines," produced by Wright Aeronautical Corp., and "Mass Production of Curtiss Pursuits," by the Airplane Division, Curtiss-Wright Corp. Approximately 80 Branch members and guests attended. After the showing of the pictures, officers of the Branch for the next year were nominated. Final elections will be held at the last meeting of the school year.

**Spartan School of Aeronautics.** A meeting was held on March 24 at which time R. Wayne Lowe was elected Chairman and G. F. Kreitzberg, Secretary. Various technical topics were discussed. Fred S. Kramer, M.I.Ae.S., is Faculty Adviser for this group of 24 Student Members.

## Personnel Opportunities

The Personnel Bureau serves individual members, as well as organizations seeking to employ aeronautical specialists. Any member or organization may have requirements listed without charge.

*Wanted*

**Aeronautical Engineer** to organize, supervise, and teach Engineering Defense Training courses in Dallas and Fort Worth, Texas, in program sponsored by The University of Texas. College degree, industrial and teaching experience desirable. Salary $300 per month or more, depending on qualifications. Send applications with complete personal history and photograph to M. J. Thompson, The University of Texas, Austin, Texas.

**Instructors** (two) familiar with airplane design, salary $2,200 a year; **Research Assistants** (two) with no teaching duties, familiar with aerodynamic research, stipend $900 plus income from research work, opportunities for graduate work; **Teaching Assistants** (three) in engine, structural and aerodynamic laboratories, stipend $900 first year, opportunities for graduate work; **Fellow** for specialized research, no teaching duties, stipend $750, opportunities for graduate work, appointment June 15. Location east with large university. Give educational background, professional experience, photograph, in letter of application. Address reply to Box 150, Institute of the Aeronautical Sciences.

**Approved Aircraft School** in midwest desires mechanic and engineering instructors. Furnish qualifications, experience and snapshot in first letter. Address reply to Box 152, Institute of the Aeronautical Sciences.

**Airplane Designers, Stress Analysts, and Draftsmen** needed for few vacancies remaining on engineering staff. At least four years' experience essential. Release will be required if now employed in similar position. (Can also use one or two recent graduates for computation work.) Write for appointment stating education, experience, and salary. Snead & Company, Aeronautical Division, 350 Communipaw Ave., Jersey City, N. J.

**Aeronautical Engineer.** Large corporation converting to aircraft construction requires services of aeronautical engineer experienced in design and production. Prefers man experienced in plywood aircraft construction and capable of directing the engineering staff. Please give details of experience, age, draft status, educational background, and salary requirements. Address reply to Box 154, Institute of the Aeronautical Sciences.

**Aeronautical Engineer** experienced in plywood aircraft manufacturing wanted by southern aviation company. Must be able to take active charge of manufacturing and engineering operations. State experience and salary expected in first letter. Address Aviation Engineering, Inc., 1390 Blashfield Street, S.E., Atlanta, Ga.

**Assistant Professor** to teach courses in aeronautical engineering and assist in mechanical engineering. Salary $2,600 and up according to qualifications. Application should give education and experience and state salary expected. Address reply to L. D. Hayes, Head, Department of Mechanical Engineering, West Virginia University, Morgantown, West Virginia.

**Six draftsmen** preferably with instrument experience for work on confidential projects for Army and Navy having vital bearing on the War effort. Applicants must be able to satisfy F.B.I. regarding loyalty prior to starting work. Residence and work will be in small town on Long Island. It is anticipated work will be permanent. Address reply to Box 157, Institute of the Aeronautical Sciences.

*Available*

**Aeronautical Engineer** (B. of Ae.E.) with five years' experience in aircraft power plant installation design, including layout, supervision, shop contact, liaison, and field work for at least five first-rate military airplanes; also one year of shop experience as mechanic and inspector in aircraft. Desires position in supervisory design capacity with power plant accessory manufacturer or as group engineer on power plant with aircraft manufacturer. Address reply to Box 155, Institute of the Aeronautical Sciences.

**Aeronautical Engineer,** with twelve years of practical and well-rounded experience in the aeronautical design field and with the U.S. Navy. Also instructor in aircraft design. Executive and inventive ability. Hard working. Desires position with a new or expanding concern in the capacity of chief, assistant chief, project engineer, or similar. Address reply to Box 153, Institute of the Aeronautical Sciences.

**Aeronautical engineer and test pilot** desires permanent and responsible position. Extensive aeronautical research and development experience with Government and major aircraft manufacturer. Training, including Master of Science degree, at leading engineering college. Particularly qualified in development and performance flight testing as applied to power plant installation development. Able to solve new engineering problems in practical manner. Inventive ability demonstrated. Location in Southern California preferred. Age 39. Address reply to Box 156, Institute of the Aeronautical Sciences.

## Changes In Membership

The following changes in the membership of the Institute have occurred since the publication of the previous issue of the Journal.

### Transferred from MEMBER to Associate Fellow Grade

**Weining, Earl Oliver,** Project Engineer (Navy), Wichita Div., Boeing Airplane Co.

### Elected to MEMBER Grade

**Darragh, James Bard, Jr.,** B.S. in E.E.; Sr. Research Engineer, Structures, Lockheed Aircraft Corp.

**Hahn, Stuart Hamilton,** B.S. in M.E.; Mech. Engineer, Aerodynamics Dept., Airplane Div., Curtiss-Wright Corp.

### Elected to Industrial Grade

**Baughman, Harold E.,** President, Aero Publishers, Inc.

### Elected to Technical Member Grade

**Brown, Robert,** Lt., South African Air Force; Asst. to Air Attaché, South African Legation; Tech. Repr., South African Airways.

**Curr, Maurice David,** Process Engineer, Consolidated Aircraft Corp.

**Gross, Maynard Cherbo,** B.S. in Ae.E.; Engineer, Airplane Div., Curtiss-Wright Corp.

**McIver, Robert Murdo,** B.S. in Min.E.; Flight Commander, Cal-Aero Academy.

### Transferred from Student to Technical Member Grade

**Bailey, Walter Ernest,** Aero. Engineer, Platt-Le Page Aircraft Corp.

**Brattvet, Robert Wesley,** B.Ae.E.; Apprentice Engineer, Pan American Airways System.

**Colen, Donald J.,** M.S. in Ae.E.

**Crowther, Gwynn, Jr.,** Jr. Stress Analyst, Ryan Aeronautical Co.

**Engebretson, Hartwell Emil,** B.Ae.E.; Engineer, Boeing Aircraft Co.

**Ford, Lloyd Dalton,** Asst. Instructor Meteorology, Air Corps Basic Flying School, U.S. Army Air Forces.

**Freitag, Robert Frederick,** Ensign, U.S.N.R.; Asst. Engineer, Bureau of Aeronautics, Navy Dept.

**Gray, William Edwin, Jr.,** M.E.; Jr. Aero. Engineer, Langley Memorial Aero. Lab., N.A.C.A.

**Hartley, David Brooks,** Instructor, Casey Jones School of Aeronautics.

**Hittner, Richard,** Jr. Engineering Draftsman, Mitchel Field Sub-Depot, Base Engineering, War Dept.

**Middleton, James A.,** Sr. Draftsman, Lockheed Aircraft Corp.

**Myron, George Walker,** Instructor, Academy of Aeronautics.

**Potters, Stephen,** Draftsman, Republic Aviation Corp.

**Reed, Herbert William,** B.S. in Ae.E.; Instructor, Aeronautical University, Inc.

**Smith, Larz McClellan,** B.S. in Ae.E.; Engineer, Waco Aircraft Co.

**Woodall, James Franklin,** B.S. in Ae.E.; Aero. Engineer, Consolidated Aircraft Corp.

**Wright, William Fred,** M.A.


# The Technical Information Service
of the
# Aeronautical Archives
of the
# Institute of the Aeronautical Sciences

This service has experienced personnel under the supervision of trained aeronautical engineers to compile any information desired. The services range from listing specialized reference books to the preparation of exhaustive bibliographies, digesting of reports and general surveys of any aeronautical subject.

Research work is charged at the usual library fee of $2.00 per hour. Special arrangements may be made for work requiring several weeks or months.

Translators are available for accurate transcriptions of all foreign language data. Translations are carefully edited by trained engineers at the standard rate of 1¢ per word. Minimum charge, $2.00.

Reproductions of any material in the Aeronautical Archives of the Institute may be ordered at standard photostat rates.